Doctoral Dissertation
(Shinshu University)

Experimental and Numerical Study of Transitional Channel Flow

March 2013

Daisuke Seki

Experimental and Numerical Study of Transitional Channel Flow

ABSTRACT

A hot-wire measurement and direct numerical simulations were performed to investigate transitional channel flow. Aims of the investigation are to determine the transitional Reynolds number and to reveal the generation mechanism of disturbance structures.

The transitional channel flow was realized by reduction of Reynolds number (Re) of strongly disturbed channel flow. The experiment conducted by a hot-wire anemometry in a planar channel flow. From the streamwise velocity fluctuation energy and the linear extrapolation of the intermittency factor, the lower marginal Re, which is defined as the minimum Re for partial existence of sustainable turbulence, was estimated around 1400 based on the channel width and the bulk velocity. The upper marginal Re at which the intermittency factor reaches one is about 2600. The flow fields passing a turbulent patch, reconstructed with conditional sampling of the streamwise velocity data based on the time of laminar-turbulence interfaces, indicate a large-scale flow structure across laminar and turbulent parts. This large structure makes it possible for some regions to be at higher Re than the average, so that turbulence can partly generate or survive there. The moderate-scale disturbances larger than the turbulent one appear in the non-turbulent parts of the transitional flow, causing the non-turbulent velocity profile to be almost identical to the turbulent one. The large-scale fluctuation is observed even over $Re = 2600$. This leads to the conclusion that a turbulent channel flow close to the

upper marginal Re becomes inhomogeneous.

The lattice kinetic scheme which is based on a discrete particle kinetics was carried out for relaminarizing channel flow. The scheme has a simple algorithm compared to other numerical schemes so it suitable as the first onset of the numerical investigations. Lifetime of flow disturbances estimated by fluctuation energy variation increases exponentially with increasing Re, and the minimum Re was determined at the infinitesimal lifetime.

The direct numerical simulation with spectral discretization in spaces was performed for parametric tests with larger computational domain and in higher speed than the simulation with the lattice kinetic scheme. The simulation reproduced the intermittent flow with turbulent patches and streaky structures of the modulate scale in the non-turbulent regions, and was in quantitative agreement with the experimental results in terms of the intermittency factor and mean velocity profiles. The detail analysis of integrated flow fields revealed that the large-scale flow around and inside the turbulent patches is induced by blockage effect of the turbulent patches. Appearance of the streaky structures well relates to curvature of streamlines skewing by the patch blockage, strongly suggesting that the streaky structure is caused by the cross-flow instability.

ACKNOWLEDGMENTS

I would like to thank my supervisor, Prof. Masaharu Matsubara, for shearing his knowledge of fluid experiments and his deep insight of fluid dynamics and for teaching me how one of the best researcher should be.

Thanks to Profs. Junichiro Shiomi, Masato Yoshino, Shin-ichi Tsuda and Shouichiro Iio for providing useful comments to improve the thesis.

I am deeply grateful to thank Mr. Noritaka Aota who gives me heartwarming encouragement and constructive comments. It has been a really pleasure working with Mr. Aota.

Many thanks to Mr. Takeshi Okumura and Mr. Takayuki Numano for improving and assembling the air channel facility and for making the pre-experiment.

Thanks also to Mr. Yoshihiro Iwatani who has made a part of experiment in the air channel facility.

I wish to thank Mr. Tsutomu Natori, Mr. Kenta Watanabe and Mr. Shunsuke Akaoka for producing and discussing, pictures and movies of the flow visualization in the water channel facility.

Finally, but not least, I appreciate my parents for their cordial support and understanding.

Table of Contents

List of Figures

CHAPTER 1

Introduction

Transition to turbulence in shear flows such as channel, Couette, pipe flows and boundary layer has attracted many physicists, mathematicians and engineers as an intriguing issue in classical dynamics and mechanics since the pioneering pipe flow experiment by Osborne Reynolds.

Linear stability analysis for seeking exponential growth modes is conventionally utilized as the first step of a valuable method to study transition to turbulence. However, the critical Reynolds numbers for infinitesimal disturbance do not agree with experimental observations in the canonical flows. According to linear stability theory, channel flow is stable for $Re < 7696$ and Couette and pipe flows are stable for all Reynolds numbers, where Re is Reynolds number based on the bulk mean velocity and channel width. Most of experiments have shown that the channel flow undergoes transition to turbulence at much lower Re if initial disturbances are adequately strong.

The channel flow is one of the most fundamental and significant flow field in fluid dynamics and it is the simplest to deal the numerical simulation. Attempt to determine the marginal Reynolds number in a channel flow, defined the minimum for the self-sustainable turbulent flow, dates back to 1928[1], an experiment performed by Davis and White. They measured the skin friction coefficient and demonstrated that it reaches the turbulent value at $Re = 2400$. An hot-wire

anemometry, becoming the majority technique for air flows in the 1960s, made possible acquisition of rich information on flow disturbances. Badri Narayanan[2] estimate the marginal Re from the extrapolation of the streamwise decay of the fluctuations, and intermittency of the transitional channel flow was observed by Patel and Head.[3] In the 1980s, the behavior of the artificial disturbance in the channel flow is examined studiously at low Reynolds numbers. Some methods to determine the marginal Reynolds number were used, for example, a variation of skin friction[1, 3], energy variation[2] and flow visualization[4, 5, 6]. These studies except Badri Narayanan[2] show that the marginal Reynolds number exists around $Re = 1300$. Direct numerical simulations[7, 8] and flow visualization[9, 10, 11] demonstrated that laminar and turbulent regions form a much-patched pattern, and that streaky(longitudinal roll) structures appear in the laminar region.

In this study, we used two way approaches to reveal the transitional channel flow and to understand the generation mechanism of characteristic disturbances in the flow. One is by performing an experiment with hot-wire anemometry and the other is by means of direct numerical simulations. Advantages of the hot-wire measurement are the high time resolution and long sampling, and the direct numerical simulations are more suitable to investigate the disturbance structure.

The thesis is organized as follows: Chapter 2 presents the lattice Boltzmann simulation result of relaminarizing channel flow. The lattice kinetic scheme was carried out to investigate the energy variation and the half-lifetime and the analogy of relaminarizing process of pipe flow are discussed. Chapter 3 provides hot-wire measurement results of relaminarizing and transitional channel flows. The streamwise properties of the relaminarizing channel flow, intermittency factor and upper and lower marginal Reynolds numbers are presented and discussed by considering reconstructed flow fields. Chapter 4 presents direct numerical simulation by means

of a spectral method. The simulation is compared with the hot-wire measurement results for validation of the simulation. Detailed analysis of the integrated flow field carried out and the generation mechanisms of turbulent patch and streaky structure. In Chapter 5 conclusions and feature works concerning this study are stated.

CHAPTER 2

Numerical analysis using the lattice kinetic scheme

2.1 Preliminaries

In a direct numerical simulation of the transitional channel flow, the spectral method is usually used[12, 13]. Though the spectral method is highly accurate and efficient to calculate, it has disadvantage that the complicated algorithm to set the boundary condition. Since the early 1990s, the lattice Boltzmann method (LBM)[14, 15] has been developed as an alternative and promising numerical scheme for flows of viscous, multicomponent, or multiphase fluids. The advantages of the LBM over standard Navier-Stokes codes are the simplicity of the algorithm, high assurance of the mass and momentum conservation and the numerical stability. In particular, the lattice kinetic scheme (LKS)[16], an improved method of the LBM, tempts numerical researchers to save computational memory. The objective in this chapter is to investigate the relaminarizng channel flow by using the LKS.

2.2 Numerical method

Non-dimensional variables in the formula in the LKS are defined based on a characteristic length, L, a characteristic particle speed c, a characteristic time scale t_0

and a reference density ρ_0[15]. The three-dimensional 15-velocity model is given by the following equation:

$$
\begin{aligned}
&[\boldsymbol{c}_1, \boldsymbol{c}_2, \boldsymbol{c}_3, \boldsymbol{c}_4, \boldsymbol{c}_5, \boldsymbol{c}_6, \boldsymbol{c}_7, \boldsymbol{c}_8, \boldsymbol{c}_9, \boldsymbol{c}_{10}, \boldsymbol{c}_{11}, \boldsymbol{c}_{12}, \boldsymbol{c}_{13}, \boldsymbol{c}_{14}, \boldsymbol{c}_{15}] \\
&= \begin{bmatrix}
0 & 1 & 0 & -1 & 0 & 0 & 0 & 1 & 1 & -1 & -1 & 1 & 1 & -1 & -1 \\
0 & 0 & 1 & 0 & -1 & 0 & 0 & -1 & 1 & 1 & -1 & -1 & 1 & 1 & -1 \\
0 & 0 & 0 & 0 & 0 & 1 & -1 & 1 & 1 & 1 & 1 & -1 & -1 & -1 & -1
\end{bmatrix}.
\end{aligned} \tag{2.1}
$$

In the LKS, the fluid density ρ and fluid velocity $\boldsymbol{u}$ at a point $\boldsymbol{x}$ at time t are derived by following equations:

$$
\rho(\boldsymbol{x}, t) = \sum_{i=1}^{15} f_i^{\mathrm{eq}}(\boldsymbol{x} - \boldsymbol{c}_i \Delta x, t - \Delta t) \tag{2.2}
$$

$$
\boldsymbol{u}(\boldsymbol{x}, t) = \frac{1}{\rho(\boldsymbol{x}, t)} \sum_{i=1}^{15} \boldsymbol{c}_i f_i^{\mathrm{eq}}(\boldsymbol{x} - \boldsymbol{c}_i \Delta x, t - \Delta t), \tag{2.3}
$$

where Δx is a spacing of the cubic lattice and Δt is a time step. The equilibrium distribution function f_i^{eq} is obtained by

$$
\begin{aligned}
f_i^{\mathrm{eq}} &= E_i \rho \left[1 + 3 c_{i\beta} u_\beta + \frac{9}{2} c_{i\beta} c_{i\gamma} u_\beta u_\gamma - \frac{3}{2} u_\beta u_\beta \right. \\
&\quad \left. + A \Delta x \left(\frac{\partial u_\gamma}{\partial x_\beta} + \frac{\partial u_\beta}{\partial x_\gamma} \right) c_{i\beta} c_{i\gamma} \right],
\end{aligned} \tag{2.4}
$$

where $E_1 = 2/9$, $E_i = 1/9$ $(i = 2, 3, \ldots, 7)$, $E_i = 1/72$ $(i = 8, 9, \ldots, 15)$, and β, γ represent Cartesian coordinate with the summation convention and subscript i indicate the directions of the 15-velocity model. Note that the time step Δt is chosen as a time during witch the particles travel the lattice spacing; it follows that $\Delta t = \mathrm{Sh} \Delta x$ where $\mathrm{Sh} = U/c$ is the Strouhal number.

The pressure p is related to the density ρ by the following equation:

$$
p = \frac{\rho}{3}. \tag{2.5}
$$

The kinematic viscosity ν of the fluid is related to A and Δx as follows:

$$\nu = \left(\frac{1}{6} - \frac{2}{9}A\right)\Delta x. \tag{2.6}$$

The following finite difference approximation is used to calculate the first derivatives of fluid velocity in the equilibrium distribution function f_i^{eq}:

$$\frac{\partial u_\gamma}{\partial x_\beta} \approx \frac{1}{10\Delta x}\sum_{i=2}^{15} c_{i\beta} u_\gamma(\boldsymbol{x} + \boldsymbol{c}_i\Delta x, t) \tag{2.7}$$

The coordinate system is defined as the streamwise direction x, the spanwise direction y and the wall-normal direction z, respectively. Velocities, spatial positions and time in this chapter are normalized by the channel half-width δ and the mean center velocity U_{CL}, and the bulk Reynolds number is defied as $Re_{CL} = U_{CL}\delta/\nu$. The computational domain is $12.56\delta \times 6.24\delta \times 2\delta$ in x, y, z and it is discretized into a $314 \times 156 \times 50$ cubic lattice. Periodic boundary conditions are used in the x and y directions and non-slip boundary condition is adopted on the walls. A pressure difference between the inlet and the outlet is adjusted at every time step so that mass-flux in the channel is constant.

2.3 Result and discussion

The initial condition to simulate a fully developed turbulent flow at $Re_{CL} = 3000$ is used to the sine wave disturbance whose amplitude is $0.04\,\%U_{CL}$ within the whole domain except the rigid walls. Figure 2.1 and 2.2 shows the mean velocity and velocity fluctuation profiles at $Re_{CL} = 3000$ at a steady state where Re_τ is a Reynolds number based on the skin friction velocity and channel half width δ. $u_{x,\mathrm{r.m.s.}}$ has the peak at near the wall and more large value than the others. The characteristic of turbulent flow is captured in present calculation. Nevertheless, the quantitative agreements for previous works[12, 17] are not seen. Furthermore,

comparing the DNS [18], the LKS mean profile is laminar-like despite the higher Reynolds number. Though these inconsistencies seems to be caused by lack of the spatial resolutions and the small computational box, it seems that disturbances in the flow are strong enough to realize the transitional flow after the Reynolds number reduction. Therefore, this flow was used as initial condition for following calculations.

The relaminarizing flow is realized by increasing the kinematic viscosity instantaneously and the range of Reynolds number is $Re_{CL} = 600$ to 1230. Hereafter, the non-dimensional time is measured from the time at the increase of the viscosity.

As seen in the Figure 2.3, the fluctuation energy indicates the exponential decay with the time and also the slope of the energy variation becomes more gradual with increasing Reynolds number. The reason is that the energy dissipation becomes the low since the flow sustainable the turbulence more easy with increasing Reynolds number. The similar phenomenon is also observed in the pipe flow experiments by Pexinho and Mullin[19]. They based on the streamwise decrease of the observation probability of equibrium puffs to estimate the half-life. In both cases, the half-life decreases exponentially with increasing Re_{CL} to zero. Figure 2.4 shows the snapshot of relaminarizing flows at $Re_{CL} = 600$ and 1230, at $t^* = 50, 250, 500$. The fluctuation gradually decreases with time and flow undergoes to laminar at $Re_{CL} = 600$, and the fluctuation almost disappears at $t^* = 600$, while at $Re_{CL} = 1230$, the velocity fluctuation is sustained at the same time.

Relation between the inverse of half-lifetime τ^{-1} and Re_{CL} shows at Figure 2.5. The half-lifetime τ is defined as time for the fluctuation energy to decay to half of the initial disturbance energy. The τ is calculated from the energy growth rate which estimated as exponent of the least square fitting. In Figure 2.5 (a) , τ^{-1} is decreasing exponentially with increasing Re_{CL} in range of $Re_{CL} = 600$–1230 and it

asymptotic to 0. To compare, a experimental result of the pipe flow [20] shows at Figure 2.5 (b) . The tendency is similar to the present result suggesting that the relaminarizing process of each flow case may have similarity. But, at more higher Re cases the estimation of τ becomes uncertain, therefore to decide the function of to describe the behavior the lifetime requires the more careful analysis.

2.4 Summary

The lattice kinetic scheme based on lattice Boltzmann method has been applied to the simulation of the relaminarizing channel flow. The turbulent energy indicates an exponential decay for $600 \leq Re_{CL} \leq 1230$.

Also, the energy lifetime is estimated and found that it increases exponentially with the Reynolds number. These results indicate that process of relaminarization in a channel flow has analogy with that in a pipe flow.

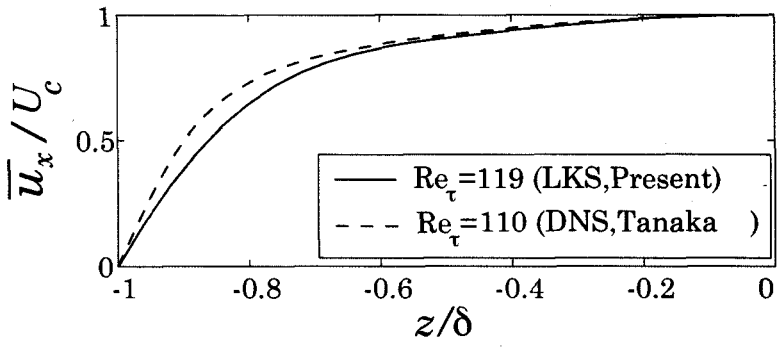

Figure 2.1: Mean velocity profiles: —, present results; - - -, DNS results by Tanaka et al[18].

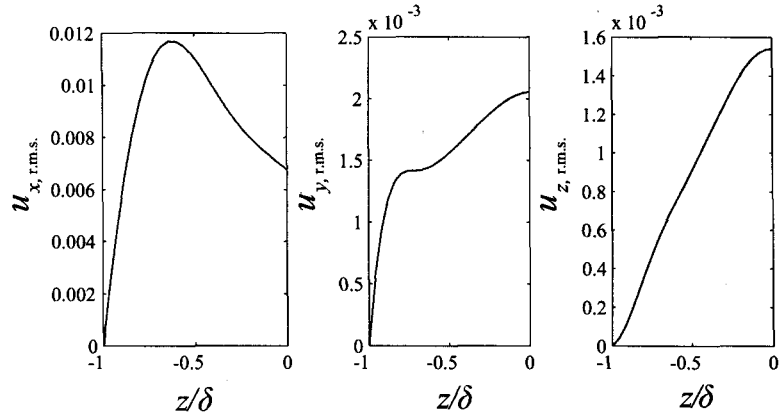

Figure 2.2: Root-mean-square (r.m.s.) values of streamwise, spanwise and wall-normal velocities.

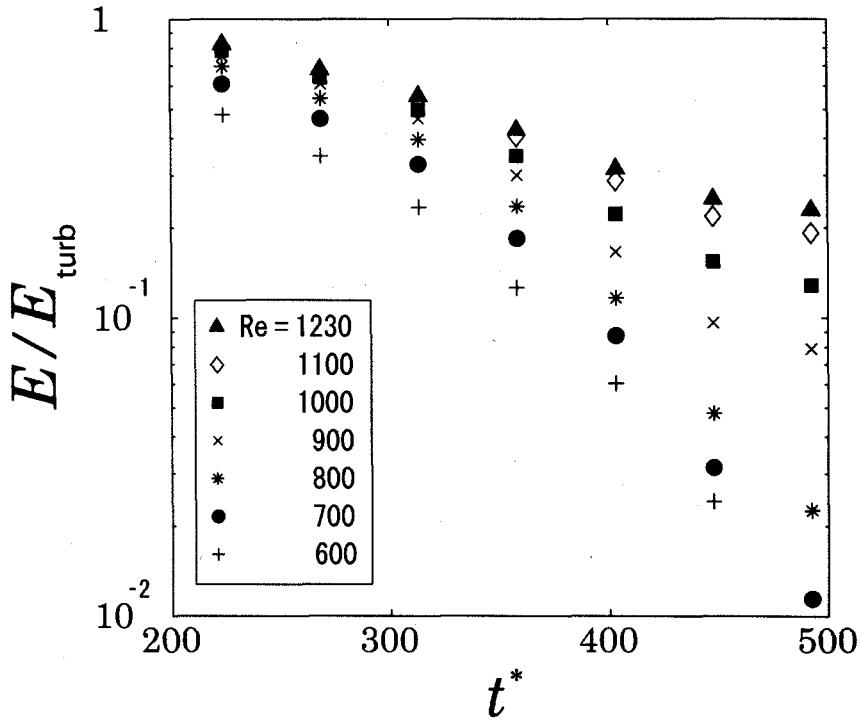

Figure 2.3: Time variation of turbulent energy for different Reynolds numbers ($600 \leq \mathrm{Re} \leq 1230$). The data are plotted on semi-log scales ($t^* = tU_c/\delta$).

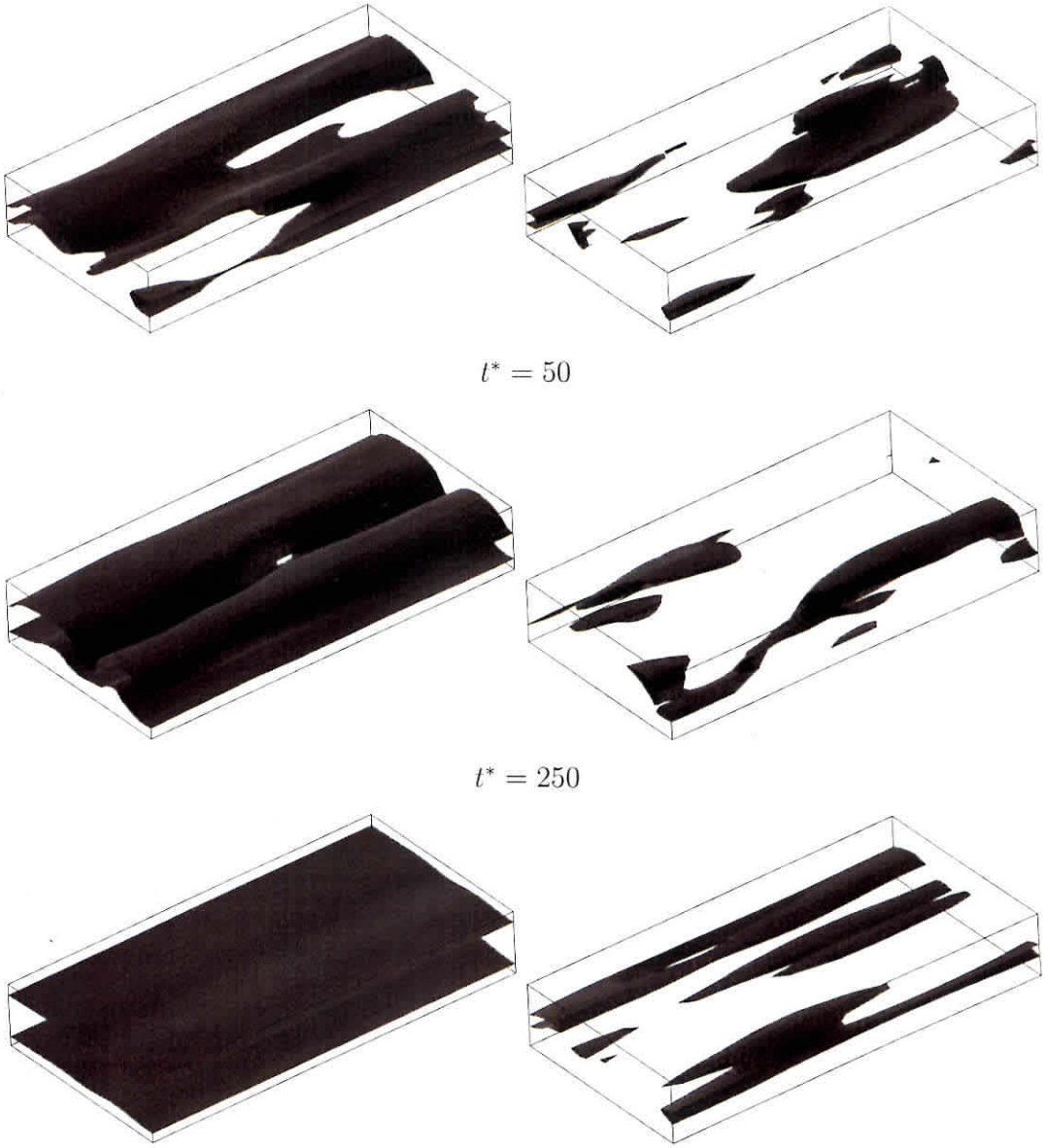

Figure 2.4: Time evolution of iso-surface of streamwise velocity ($|u_x| = 0.013$ and 0.027) in the relaminarization for different Reynolds number: (a) Re = 600; (b) Re = 1230 ($t^* = tU_c/\delta$).

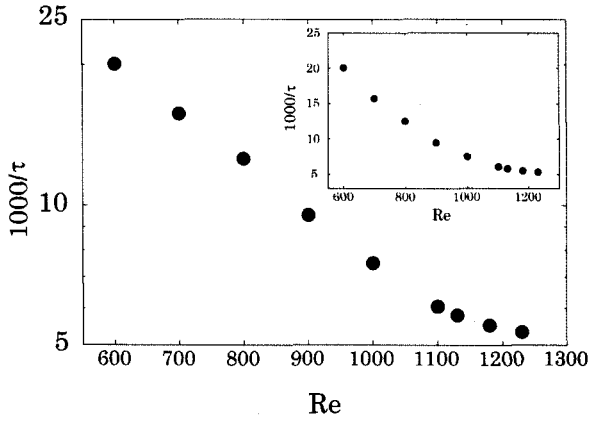

(a)

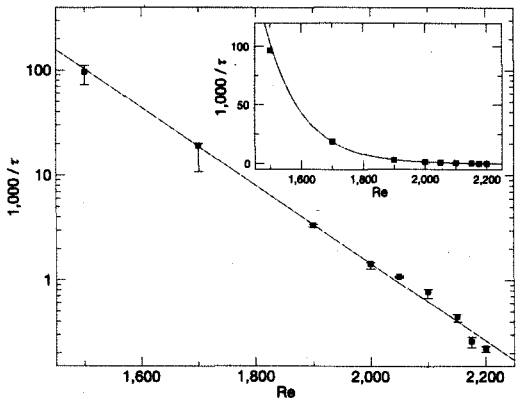

(b)

Figure 2.5: Relation between halflife and Reynolds number: (a) Present result in channel flow; (b) Numerical result in pipe flow by Hof et al[20].

CHAPTER 3

Experimental investigation of relaminarzing and transitional channel flows

3.1 Preliminaries

Determination of the marginal Reynolds number (Re), at which shear flow can barely sustain a state of turbulence, is one of the classic subjects of fluid dynamics. In such an extreme condition, systems of disturbance preservation would be distinct, and would probably maintain at a much higher Re. Hence, knowledge about the ultimate sustaining system would shed light on the physics of turbulent shear flows. According to the linear stability analysis for a laminar channel flow, any infinitesimal amplitude disturbance decays under the critical Re 7696 based on the bulk (mean) velocity and the channel width. [21] Even below the critical Re, however, the flow becomes turbulent if the initial disturbance is sufficiently strong.

One of the primary studies of the subcritical turbulent channel flow was done by Davies & White [1] with a stiff water channel facility. Though they did not discuss inlet disturbance in their paper, a sidewall of the channel inlet in the test facility they used had a sharp corner that could cause strong initial disturbances. Their precise pressure drop measurement with various flow rates and channel widths indicates the local minima of the skin friction coefficient at $Re = 1440$ and reaches the

turbulence value at $Re = 2400$. The fact that the marginal Re is much lower than the critical Re for an infinitesimal disturbance leads to the conclusion that there exist two states of flow between the two Re values. If the initial disturbance is high enough to excite sustainable turbulent disturbances, the flow over the marginal Re becomes turbulent. To determine the marginal Re, one must control the initial disturbance to be at a relatively high level.

Patel & Head[3] investigated pipe and channel flows around a transitional Re by means of a hot-wire anemometer and a flattened Pitot tube. They introduced sufficient disturbance to induce a transition to turbulence with the sharp corners at the channel entrance and additional wire tripping across the entry. They observed intermittent flow with turbulent bursts in the range of $Re = 1380$ to $Re = 1800$, while agreement of the skin friction with the -1/6 power law appears at the much higher $Re = 2800$. Badri Narayanan[2] measured velocity fluctuations in a sub-critical channel flow following a fully developed turbulent flow and estimated the marginal (what he termed 'critical') $Re = 2800 \pm 100$ from extrapolation of the streamwise decay of the fluctuations. Nishioka & Asai[6] performed a hot-wire measurement in a channel flow strongly contaminated by cylinder-generated vortical disturbances as well as a periodic jet from a wall hole, and they observed a burst appearance at $Re = 1330$ or above. Below this Re they observed only low-frequency fluctuation far downstream from the disturbance source. Carlson et al.[4] investigated natural and artificial turbulent spots in the range of a transitional Re with flake particle flow visualization and found that the spot could be generated by an artificial disturbance at or above Re of about 1330. They observed strong oblique waves at the sides and the rear of turbulent spots, and spots splitting into two spots downstream, with their gap filled with longitudinal structures. The fully turbulent flow was detected over about $Re = 2000$. Alabyoon

et al.[5] performed visualization of a turbulent spot and they could not generate a turbulent spot below $Re = 1470$. They also confirmed the oblique waves and the spot splitting, though the front and rear propagation velocities were higher than estimations by Carlson et al.[4]

These experiments on transitional channel flow indicate that the marginal Re is in the vicinity of 1400, except in the experiment by Badri Narayanan. Numerical studies are consistent with this value, such as that by Orszag & Kells[13], who performed direct numerical simulations (DNS) for strongly disturbed channel flow. Though their calculation domain and spectral modes were limited, they confirmed the sustainable non-laminar flow at $Re = 1667$, while a channel flow at $Re = 667$ showed relaminarization. As another example, a detailed numerical calculation of the transitional channel flow was performed by Iida & Nagano[22] who revealed that at $Re = 1720$ the flow was unsteady in terms of the total skin friction in the whole domain.

Groups including the present authors[9, 11] conducted flow visualization in the transitional channel flow and revealed that the transitional flow was intermittent, with laminar regions, turbulent patches and large-scale vortices in the non-turbulent regions whose typical streamwise length was 25 channel widths. They also observed laminar flow below $Re = 1200$ and turbulent flow uniformly filled with small eddies at $Re = 2500$. Fukudome et al.[7] recently performed a direct numerical simulation in a large computation box with streamwise and spanwise periodic boundary conditions and found that the patch of turbulence forms a quasi-steady diagonal band. This type of turbulent band was also reported in the direct numerical simulation by Tsukahara et al.[8]

In spite of mathematical difficulties, non-linear analyses of disturbance in the shear flows around the marginal Re were vigorously performed for the last few

decades. Recently, a new concept, 'edge state' was proposed [23, 24, 25, 26, 27, 28] and successfully described behavior of the non-linear disturbances in the transitional pipe flow.[29, 30, 31]

When considering the marginal Re, one can examine the largest vortical scale of turbulent disturbances in the wall unit. Asai & Nishioka,[32] presenting their experimental results in a transitional boundary layer, pointed out that the spanwise scale of the hairpin vortices was about 50 in the wall unit at the marginal Re and quickly increased to 100 downstream. Alfredsson & Matsubara[33] proposed that the largest longitudinal vortex should have a spanwise size larger than 50 wall units but should not exceed the geometrical limitation of the flow. This hypothesis well predicted the marginal Re values for several canonical flows.

3.2 Experimental Setup and Data Evaluation Technique

3.2.1 Air Channel Facility

The experiments were performed in an air channel facility (Figure 3.1). The air pressurized by a frequency-controlled blower gushes from a perforated pipe positioned in a settling chamber with a cross section of 190 mm × 170 mm. A two-dimensional nozzle with a contraction ratio of 34 : 1 is followed by channel entrance, expansion and test sections whose wall distance, d^*, is 5.01 mm. The entrance section is 1000 mm long and 190 mm wide. Two tripping wires of 0.5 mm diameter are strung in the spanwise direction 1 mm apart from each wall at 100 mm downstream from the outlet of the nozzle. These wires trigger a transition to turbulence, and the flow becomes a fully developed turbulence flow at the end of the entrance section. In the 1000 mm long expansion section, the spanwise distance between the channel end walls is symmetrically widened to be 260 mm at the downstream end,

so that the streamwise mean velocity drops to 73 % of the entrance mean velocity in the expansion section. The 2° tilt of the end wall is low enough to prevent flow separation. The test section following the expansion section is 2800 mm long, and its downstream end opens to the atmosphere. The idea of the end wall tilting for reducing the Re downstream of a fully developed turbulent channel flow originated from Badri Narayanan.[2]

The coordinates are defined as x, y and z, in the streamwise, wall-normal and spanwise directions, respectively, with the origin at the inlet of the test section on one of the channel walls. All non-dimensional values are based on the wall distance d^* and the bulk (mean) channel velocity U_b^*, and the the bulk Re of the channel flow is defined as $Re = U_b^* \, d^*/\nu^*$ with the air kinematic viscosity, ν^*. Dimensional values in the present paper are denoted with a superscript of ()*.

3.2.2 Measurement Technique

A constant-temperature hot-wire anemometer with a single sensor probe was used for the streamwise velocity measurements. The sensor part of the probe is made of platinum wire 1.5 mm long and 2.5 μm in diameter. Before every set of measurements, velocity calibrations of the anemometer were done in a jet potential core from an axial nozzle connected to the blower for the main channel facility. King's law modified for low velocity [34] was used for the calibration curve fitting. The temperature variation during the taking of a set of the measurements was monitored to ensure that the temperature drift of the flow from the calibration did not exceed more than 0.7 °C.

The voltages of the hot-wire anemometer were acquired via an analog/digital converter with a sampling frequency of 20 kHz, and a sampling time of 30 s for

a streamwise positioning measurement and 300 s for a detailed measurement at the most downstream position. A wedge mechanism modeled on that used by Klingmann[35] was employed for probe positioning in the wall-normal direction. It was attached at the ends of two 2300 mm long bars and was moved by a linear actuator in the streamwise direction. Accuracy of the wall-normal probe movement was checked by the parabolic Poiseuille profile below $Re = 1000$. For estimation of the wall position, we employed the symmetric property of the velocity profile for each probe traversing the channel in the streamwise direction.

During each experiment, a hygrometer and a barometer monitored the relative humidity and the atmospheric pressure in the room, respectively. The density and the kinematic viscosity of the flow were calculated from the flow temperature, the relative humidity and the atmospheric pressure.[36]

Before performing the main experiments, we measured the bulk mean velocity, U_b^*, and the wall distance, d^*, to assure the accuracy of the bulk Re. The wall distance was measured with an ellipse gauge whose rotation angle was calibrated in advance. The distance ranged from 5.00 mm to 5.02 mm with the mean of 5.01 mm chosen for d^*.

For U_b^*, we obtained the channel mean velocity, U_m^*, from integration of the time-mean velocity profile $U^*(y^*)$ over the channel width using the even tenth-order polynomial function symmetric with respect to the channel center as a fitting function. The accuracy of U_m^* was not high enough to determine the bulk Re because of hot-wire sensibility to temperature and integration error, so the nozzle pressure drop, ΔP^*, was calibrated to U_m^*, and then the relation between the bulk velocity U_b^* and ΔP^*,

$$U_b^* = \sqrt{0.3791 \frac{\Delta P^{*1.112}}{\rho^*}}, \tag{3.1}$$

was obtained, where ρ^* is the air density. This U_b^* was adopted for calculating the bulk Re, while the velocity data measured by the hot-wire anemometer were divided by U_m^* initially, as we expected this would cancel the hot-wire calibration error by the temperature drift.

3.2.3 Procedure for sorting the flow into laminar and turbulent parts

The intermittency factor, γ, which is a ratio of total time of turbulence to overall duration, represents a direct index of transitional flows in which there coexist laminar and turbulent parts. In addition, the statistics for each of the laminar and turbulent parts are very valuable for scrutiny of an intermittent flow. The procedure for dividing the flow into laminar and turbulent parts based on the velocity signals has been proposed by Hedley & Keffer,[37] Kuan & Wang [38] and others. Hedley & Keffer[37] discussed the difficulties in evaluating the intermittency factor and summarized many of the different detector functions. The greatest difficulty is determination of the thresholds for the detector functions, because they essentially affect the intermittency factor. Kuan & Wang[38] proposed a further refined technique, the so-called "dual-slope method," which determines the thresholds without ad-hoc adjustment.

The first step of the procedure we followed was selecting the detector function that can respond to the turbulence appearance. In our analysis, the sum of a term including the second time derivative and the square of the first time derivative of the streamwise velocity u, is proposed as the detector function, as follows:

$$D(t) = \left(\frac{\partial u}{\partial t}\right)^2 + \left|(u - U)\frac{\partial^2 u}{\partial t^2}\right|, \tag{3.2}$$

where t is the time, U is the time mean of u and $|\ |$ denotes the absolute value. The reason for this choice is that the function D is very rarely zero while the velocity

signal is highly fluctuated, though each of the terms individually takes zero. In addition, this detector is constant in time if the signal is a pure sine function, and the higher the frequency, the higher the value of the detector. Before calculation of the derivatives, high-frequency noise was removed from the streamwise velocity time signal by a 5 kHz low-pass filter that corresponded to a length scale of about 20% of the wall distance. We used a fast Fourier transform for the noise filtering and the derivative calculation.

Next, the complementary cumulative distribution function of the detector, D, with respect to threshold θ,

$$C(\theta) = \text{Prob}(D(t) \geq \theta), \tag{3.3}$$

was plotted in a log-linear graph. For the dual-slope method, an intersection of two different slopes of the semi-log plotted C was utilized for intermittency factor estimation. However, we found that this method was not functional for the present data, because moderate-scale fluctuation larger than the turbulence scale rounds the corner where the laminar and turbulence slopes meet. Thus we applied a single-slope method instead of the dual-slope method. This method utilizes the straight slope in high amplitude range of the detector function with a horizontal axis of $\theta^{2/3}$ instead of θ, as shown in Figure 3.2. The ordinate intercept of the slope, shown by a solid triangle, indicated a tentative intermittency factor, γ_t. The applied threshold θ_s, shown by an open triangle, was chosen so that the complementary cumulative distribution function at θ_s equals γ_t. The slope was estimated in the range $0.1\,\theta_P < \theta < 0.5\,\theta_P$, where θ_P is defined as $C(\theta_P) = 1/600000$. Though we cannot explain why C has a straight slope with $\theta^{2/3}$, the slope exists regardless of the wall-normal position and Re. Furthermore, we confirmed with human-eye checking of the velocity traces that the ordinate intercept of the slope was appropriate as the intermittency factor.

Applying the threshold θ_s yields the tentative indicator function I', that is, Blanks for $I' = 0$ shorter than three in the non-dimensional time U_b^*/d^* are filled, and then continuous parts for $I' = 1$ shorter than six are discarded. The conclusive intermittency factor γ is obtained as

$$\gamma = \frac{1}{T}\int_0^T I \, dt, \tag{3.4}$$

where I is the conclusive indicator function after filling and discarding clusters, and T is the measurement time. In the present paper, the flow state when $I = 0$ is nominally called the 'laminar part' as the counterpart to the turbulent part, though there sometimes exist strong disturbances in the laminar part.

3.3 Relaminarizing channel flow

When the Re of the channel flow in the test section is sufficiently low, turbulent disturbances produced in the entrance section fade out when the flow goes through the expansion and test sections, and the flow becomes laminar if the test channel is long enough. In this section, experimental observations of disturbances with a hot-wire probe traversing a flow in the streamwise direction are reported focusing on the critical point for the sustainable disturbances and the streamwise change of the flow properties.

Streamwise variations of profiles of the mean streamwise velocity, U, and distributions of the streamwise velocity fluctuation, u', are shown in Figure 3.3. Before commenting on the flow in the test channel, we will check to see whether the upstream flow at the exit of the entrance section, $x = -200$ is a proper disturbed flow. The bulk Re definition here is based on the velocity in the test section, not the entrance section, so $Re = 1390$ and $Re = 2680$ correspond to $Re = 1900$ and $Re = 3670$ in the entrance section, respectively. For $Re = 2680$, the mean profile and the fluctuation distribution at $x = -200$ are almost identical to the DNS result[12] at $Re = 5600$, suggesting that the flow at the end of the entrance section is the fully developed turbulent flow. The upstream mean profile at $Re = 1390$ is similar to the downstream mean profile at $Re = 1940$, though the upstream fluctuation distribution is somewhat lower than the downstream one at $Re = 1940$.

We consider the difference in the upstream conditions to be the cause of this deviation. The spectra of the velocity fluctuations at both Re values, not shown here, are widely spread in the high-frequency region. In conclusion, the velocity fluctuation in the upstream flow has sufficiently high and broad spectral components as the upstream disturbance for the purpose of the present experiment.

The downstream profiles at $Re = 1350$ are similar to the laminar parabolic profile. The profiles at $Re = 1520$ are almost constant downstream of $x = 300$. The profiles remain constant downstream of $x = 100$ for $Re = 1940$ and they are very similar to a turbulent profile in terms of a flattened profile around the channel center and a high shear near the wall. For $Re = 1350$ the wall-normal distributions of the streamwise velocity fluctuation are flat and monotonically decay except for the distribution at $x = 100$, which has a weak peak near the wall. The wall peak is more remarkable at $Re = 1520$ at $x = 100$. The downstream distributions are flat and rises at $x = 500$. There are no remarkable change of the fluctuation distributions at $Re = 1940$.

The premultiplied power spectra maps shown in Figure 3.4 reveal the dependence of the flow properties on the streamwise distance. The non-dimensional frequency is defined as $f = f^* d^* / U_b^*$. The channel center spectra map at $Re = 1350$ has a peak around $f = 0.025$ upstream, and it shifts slightly toward a lower frequency downstream with the overall energy going down. At $Re = 1440$, the peak value recovers downstream, and then at $Re = 1520$ it increases from $x = 200$ to $x = 400$. The peak frequency at the most downstream position is about 0.013 for $Re \geqslant 1440$. The equivalent length scale to this peak frequency is 80 d^* which is much larger than typical scales of the turbulent disturbance. Considering the facts that the low-frequency peak is mainly observed in the transitional flow, and that the scale is equivalent to the turbulent patch interval observed in the flow visualization, [4, 9, 11] it appears that this low-frequency peak is the result of turbulent patch passing.

The energy spectra maps near the wall in Figure 3.4 (d), (e) and (f) have a peak at a high frequency of about 0.05. Except for the fully turbulent flows, this peak is observed in the maps at $y = 0.1$ in the whole measurement cases, i.e.

$1180 \leq Re \leq 2360$, $100 \leq x \leq 500$. According to the flow visualization,[9, 11] this scale is larger than the turbulent disturbance scale, but smaller than that of the turbulent patch passing. The disturbance of this scale will be discussed below. It is notable that the peak value recovering at $Re = 1440$ is simultaneous with that in the channel center spectra map. For $Re = 1520$, the streamwise variation of the spectra near the wall is roughly constant.

The streamwise variations of the total energy, E, are shown in Figure 3.5. E was obtained with the trapezoidal numerical integration of the square of the streamwise velocity fluctuation from $y = 0.1$ to 0.5, and normalized with that at $x = 100$, E^*_{100}. At $Re = 1210$, the energy decreases downstream of $x = 100$, and the decay rate of energy gets slower downstream. With increasing Re this slowdown is more remarkable, and then at $Re = 1440$ the energy starts to rise around $x = 400$. Above or at $Re = 1700$, the streamwise energy variation keeps almost constant downstream of $x = 200$.

The velocity fluctuation energy at $x = 500$ is higher than that at $x = 100$ for $Re \geq 1520$, so that the flow seems to recover downstream at least superficially. Considering the facts that the energy for $Re \leq 1350$ still decays at the most downstream position, $x = 500$, and that the level of the energy there is very low, the flow has a very little chance to recover to a flow state with a sustainable disturbance. We made sure that the profiles of the mean velocity had no remarkable change downstream of $x = 300$ in the present Re range, $1210 \leq Re \leq 2660$. For $Re \leq 1350$ the velocity fluctuation downstream of $x = 200$ monotonically decreases, keeping its distribution. Therefore, we infer that the test channel length, $x = 500$, is sufficient for investigation of the transitional and relaminarizing channel flows, except for very close to the marginal Re.

From the streamwise energy variations we tried to judge if the flow is recovering

or not. A simple way is to fit linear lines to the downstream variations in Figure 3.5, but the inclinations of the lines depend on the streamwise range for the fitting. To avoid this arbitrariness, we tested two-term functions. We chose the simple addition of two exponential terms of x with the slow growth rate α_1, the rapid growth rate α_2 ($|\alpha_1| < |\alpha_2|$) and their coefficients A_1 and A_2 as follows:

$$E = A_1 e^{\alpha_1 x} + A_2 e^{\alpha_2 x}. \tag{3.5}$$

The addition of two power functions with exponents β_1 and β_2 ($|\beta_1| < |\beta_2|$) as

$$E = B_1 x^{\beta_1} + B_2 x^{\beta_2}, \tag{3.6}$$

and the combination as

$$E = C_1 e^{\alpha x} + C_2 x^{\beta}, \tag{3.7}$$

were also tested for the fitting. Acceptable fitting for the combination function was achieved with an rapid exponent α so that this α was manually restricted as the rapid growth rate by choosing the best-fitted growth rate for upstream region $x \leq 250$ for the initial value of iterative finding. Figure 3.5 indicates that the fitting curves of Eqs. (3.5) and (3.7) are appropriate for $Re \leq 1520$, where the energy has initial decay. However, the curve Eq. (3.6) evidently deviates from the measurements. The fittings with the power term for the rapid decay are inappropriate, independent of the formula of the slow term. This is sharp contrast to those with the exponential function. On the other hand, the validity of the formulae for the slow term is not decidable. The fact that the exponential function properly captures the rapid energy decay suggests that the dominant disturbance at the beginning of the energy decay has linear modal properties.

The Re dependence of the exponential coefficients and the exponents are shown in Figure 3.6. The sign of the slow growth rate, α_1, switches around $Re = 1400$,

while the rapid growth rate, α_2, is below zero in the range of the present estimation. The neutral growth, i.e., $\alpha_1 = 0$, is estimated at $Re = 1395$ with the linear fitting of the five measured points near the intercept. This value is one of the criteria for a flow state, laminar or not, from the energy sustainment. The exponent β for the mixed function fitting intersects the zero level at $Re = 1390$ estimated with the four points around the intersection. The intersection of the slow exponent β_1 around $Re = 1350$ is lower than the others. The reason for this shift would be because of the poor fitting with Eq. (3.6).

Badri Narayanan[2] estimated the marginal Re from the fluctuation energy decay within $10 \leq x \leq 130$. Since the rapid energy decay occurs even when the energy recovers downstream, this streamwise distance is too far upstream for the estimation. This is the reason for his overestimation of the marginal Re.

3.4 Transitional channel flow

To obtain more precise flow statistics and conditional averages, we performed concentrated measurements at the most downstream position, $x = 500$, with the longer sampling time of 300 s.

Time traces of the streamwise velocity at the center of the channel are shown in Figure 3.7. The trace at $Re = 1290$ indicates a calm state, except for a weak undulation around $t = 200$. At $Re = 1380$, high-amplitude fluctuations are occasionally observed, but they have no high-frequency components. High-frequency bursts appear in traces at or above $Re = 1480$, indicating that turbulent and laminar regions alternately pass through the hot-wire sensor. The total duration of the high-frequency appearance increases with increasing Re, and then at $Re = 2660$, the laminar duration is hardly observed in the trace. The time traces are charac-

teristic in terms of the acceleration during the turbulent bursts and deceleration of the velocity in the laminar parts, e.g., around $t = 70$ at $Re = 1620$.

Figure 3.8 shows the intermittency γ and the shape factor H at various wall-normal positions. Since the wall-normal positions are not fixed for each measurement, the γ value for a certain position is interpolated with the closest two point values. The γ value at the channel center starts to increase at $Re = 1380$ and approaches one at $Re = 2590$. Near the wall, γ also starts to increase at the same Re, 1380, though its inclination is somewhat lower. It is noticeable that γ is roughly constant in the wall-normal direction, except near the wall. As seen in the close-up around Re = 1500, γ increases almost linearly. The intersections on the abscissa at each height position are from 1390 to 1410, estimated with extrapolating linear fits of γ in the range $1440 \leq Re \leq 1740$. Below this Re, the intermittency factor asymptotically decreases with decreasing Re. In the present measurements the intermittency factor at $Re = 1290$ goes down to 0.4%. Taking the finite length of the test channel into account, we concluded that a small amount of turbulent part can survive for a certain distance. From our measurements for the wall-normal positions from $y = 0.1$ to 0.5, the full turbulent flow is realized at $Re = 2590$.

Though there is terminological fuzziness for representative Re values concerned with transitional channel flow, in this paper we defined here "marginal Re" as the limit for turbulence sustainment, and we distinguish two situations by using the terms "lower" and "upper" for partial and whole persistence of turbulent flow, respectively. The energy decay and the interpolation of the intermittency factor indicate the lower marginal Re is 1400 ± 10. If the upper marginal Re is estimated by the criterion of 99% intermittency factor, it is approximately 2600.

The shape factor is defined as follows:

$$H = \frac{U_c \int_0^1 (U_c - U)dy}{\int_0^1 U(U_c - U)dy}, \tag{3.8}$$

where U_c is the center mean velocity. The shape factor rapidly drops from the Poiseuille profile value of 2.5 when the intermittency factor starts to increase and then slightly decreases with increasing Re. This variation is in strong contrast to the boundary layer transition due to the free stream disturbance.[39] The shape factor in the boundary layer case gradually decreases with the intermittency increasing. The shape factor of the laminar part also has a sudden drop at $Re = 1500$, while the turbulent part has no remarkable tendency with Re change. The shape factor at $Re = 2660$ is still higher than that at $Re = 5600$.[12]

The number of turbulent patches passing the sensor is counted in the indicator function of the total sampling time and is shown in Figure 3.9. The value N is the number of the patches during time interval d^*/U_b^*. The values from the reconstruction of patch-passing flow fields will be discussed below. In Figure 3.9 (a), just above the lower marginal Re the number at $y = 0.5$ sharply increases and reaches the maxima around $Re = 1800$, and it then decreases due to merging of the turbulent patches. Close to the wall, the number for $Re < 2000$ is lower than that at the center, suggesting that some turbulent patches do not reach the near-wall region.

If the patch count is plotted with the intermittency factor γ, as in Figure 3.9(b), the variation at the channel center approximately fits to the parabolic curve, as follows:

$$N = 4N_{max}\gamma(1 - \gamma). \tag{3.9}$$

This curve is derived from a simple consideration of the probability. Assuming that trials are independent durations whose state is laminar or turbulent, the number of continuous durations of the turbulent state, N, increases with an increase in the number of trials, n, as follows:

$$\frac{dN}{dn} = \gamma(1-\gamma), \tag{3.10}$$

because the intermittency factor γ is the probability of turbulence at an additional trial, and $1-\gamma$ is the probability of a laminar state at the trial just before it. This equation is simply integrated with the condition that $N = 0$ at $n = 0$, and thus,

$$N = n\gamma(1-\gamma). \tag{3.11}$$

The variations of N roughly follow this prediction but the peaks have a slight tendency to shift toward higher γ. This indicates that the turbulent patches have a tendency to separate more frequently than in the homogeneous probability case.

Profiles of the mean streamwise velocity, U, and distributions of the streamwise velocity fluctuation, u', at $x = 500$ are shown in Figures 3.10 and 3.11, respectively. For transitional Re values 1530 and 1950, the velocity fluctuation distributions in the laminar state ($I = 0$) and the turbulent state ($I = 1$) are also plotted. The fluctuations of each state are obtained based on the mean velocity of the state rather than the whole mean velocity. The mean profile at $Re = 1260$ agrees with the parabolic laminar profile indicating that the hot-wire measurement at the closest point to the wall is not influenced by additional heat flux to the wall. The fluctuation distributions are less than 5%, and considering the highly disturbed upstream condition, this fluctuation level is reasonable as a relaminarizing flow. When the Re increases to 1530, the mean velocity suddenly decelerates in the vicinity of the center, while that near the wall accelerates. The profile drastically changes between $Re = 1390$ and $Re = 1650$, and the shape factor varies as well.

It is noteworthy that the transitional and turbulent mean profiles resemble one another, except close to the lower marginal Re.

It is also remarkable that there is little difference between the mean profiles for the laminar and turbulent states at $Re = 1950$ and this similarity was observed above $Re = 1620$. The numerical simulation[7] at $Re = 1660$ also indicates that mean profiles for the laminar and turbulent parts are almost identical.

As shown in Figure 3.11, the fluctuation distributions up to $Re = 1530$ are uniform across most of the channel width. The laminar distribution at $Re = 1530$ is also uniform, while an increase near the wall appears in the turbulent distribution. At $Re = 1950$ the fluctuation rises near the wall and decreases around the center, so that the distribution becomes very close to that at $Re = 2660$. The laminar and turbulent distributions at $Re = 1950$ also have a near-wall peak, and the laminar one is slightly lower than the turbulent one. Unexpectedly, the fluctuation at $Re = 2660$ is distinctly higher than that at $Re = 5600$, suggesting extra disturbance production.

The Re dependence of the velocity fluctuation at $y = 0.5$ and $y = 0.1$ is shown in Figure 3.12. The fluctuation at the channel center is rapidly increasing around $Re = 1400$ reaches a peak at $Re = 1520$, and then gradually decreases with increasing Re. This feature of the rapid increase and the gradual decrease appears in the conditional distributions for the laminar and turbulent cases, though the increase for the turbulent part weakens. The fluctuations for the whole and laminar durations near the wall also show a rapid increase, and the whole duration nearly maintains a constant value, 0.2 for $1800 < Re < 2500$. The turbulent fluctuation near the wall is relatively high, and its Re dependence is modest. Agreements between the center and near-wall fluctuations for the whole and laminar duration in the rapid increase indicate that a uniform distribution of the fluctuation sensitively

rises just above the lower marginal Re.

At the middle of the transitional Re range the turbulent-like mean velocity profiles with the low shape factor and high fluctuation are observed, even for the laminar part. This suggests intense wall-normal exchange of the streamwise momentum comparable to the Reynolds stress in a turbulent channel flow. The velocity signal in the laminar part, however, contains no high-frequency disturbance. To seek disturbances transporting the momentum in the laminar part, we surveyed velocity spectra. Figure 3.13 is a contour map of the premultiplied frequency spectra of the streamwise velocity fluctuation at the channel center. The thick black and gray (blue) lines indicate peak positions of the spectra intensity. We note that a peak at a very low frequency is distributed in a wide range of Re with the maximum around $Re = 2100$. In the middle range of the transitional Re, these values are very close to the patch appearance, N, indicated by the light gray (aqua) line. The length scale corresponding to the peak decreases from 65 d^* to 25 d^* with increasing Re and is the same order of magnitude as the patch appearance interval investigated in the flow visualization.[9, 11] It is noteworthy that this large-scale peak at $f = 0.04$ is observable even in the full turbulent state at $Re = 2660$. In the spectral map at $y = 0.3$ shown in Figure 3.14, the high-frequency peak intensifies and the low-frequency peak is still confirmed. A new peak appears between the very low and high peaks in the low-Re region. As seen in the near-wall spectra map of Figure 3.15, this moderate-frequency peak is more distinct in a whole transitional Re range.

The velocity fluctuation energy distributions over the wall-normal direction and the Re (Re-y) are mapped with frequency filters in Figure 3.16. The total energy distribution spreads from the near-wall region to the channel center just above the lower marginal Re, and it concentrates at the near-wall region with increasing Re.

The large-scale energy was evaluated by means of low-pass filtering with a cutoff frequency $f_L = 0.04$. It is evident that around $Re = 1500$ there exists a peak at the center.

The velocity fluctuation after the band-pass filtering has a peak near the wall in the whole transitional Re range. The lower and higher cutoff frequencies are f_L and $f_H = 0.15$, respectively. The fluctuation distribution with the near-wall peak suggests disturbance generation caused by the wall-normal velocity gradient of the mean shear and the wall-normal velocity fluctuation, v', through the term $v'\partial U/\partial y$. This moderate-scale disturbance will be discussed again after the proceeding conditional sampling analysis. On the other hand, we inferred that the large-scale fluctuation peak at $Re = 1500$ was not caused by vortical disturbance, because the term could not produce high fluctuation at the channel center where $\partial U/\partial y = 0$.

The high-frequency energy whose scale corresponds to the turbulent disturbance scale is obtained from the high-pass filtered velocity fluctuation with the cutoff frequency f_H. Its wall-normal distribution is very similar to the band-pass one in terms of the near-wall peak, while the peak value increases with Re, in contrast to the constant peak value in the band-pass map over $Re = 1800$. Therefore, we conclude that this high fluctuation is due to the turbulent disturbance inside the patch.

3.5 Conditional sampling analysis around an interface between the laminar and turbulent parts

We performed conditional sampling on the basis of an interface between turbulence and laminar states to investigate the detailed properties of the flows around the

interface. The streamwise velocity is conditionally sampled with a reference time at the flow state switching from laminar to turbulent (LT), or from turbulent to laminar (TL). The samples are restricted by the length of the pure laminar or turbulent flow state. We confirmed that this restriction has no significant influence on the conditionally sampled results if it is longer than 10 d^*/U_b^*, and we thus fixed the minimum length of the pure flow state at N^{-1} of the channel center, which is always much longer than 10 d^*/U_b^* (see Figure 3.13).

Figure 3.17 shows the time variations of the local (or temporal) Reynolds number, Re_s, which is calculated by means of integration of the conditionally averaged velocity with the tenth even polynomial fitting the same as the estimation of the bulk mean velocity. The differential time, Δt, is measured from the reference time at the interface. Rough similarities of variations of Re_s around the laminar-turbulent interfaces are illustrated when Re_s is divided by Re. In the variation of LT, the Re_s rapidly increases just after the minimum at the interface time ($\Delta t = 0$), up to the local maximum around $\Delta t = 1$, and after short reduction it increases again. Just before the interface time, Re_s decreases but not as rapidly as the turbulence side, and before the mild variation around $\Delta t = -5$ it constantly decreases. The far laminar side slope around $\Delta t = -10$ becomes steeper as the bulk Re increases, and the extrapolated values at the interface time ($\Delta t = 0$) are about $Re_s/Re = 0.96$ independent of Re. On the other hand, the far turbulence side slopes keep a constant inclination, and their extrapolated value at $\Delta t = 0$ drops from 0.95 to 0.92 with increasing Re. Variations of Re_s/Re for the interface TL (Figure 3.17 (b)) have valleys just before they reach peaks at the interface time. There also exist local maxima before the minima following the long slope of Re_s on the turbulent side. After the peaks at the interface time, Re_s monotonically decreases, with slowing around $\Delta t = 4$. The laminar and turbulent slopes apart from

the interface have the same dependence on Re as in the LT case. The extrapolated values of the far laminar slopes at the interface time are about $Re_s/Re = 1.14$ regardless of Re and those of the far turbulent slopes increase from 1.10 to 1.14 with increasing Re.

The far slopes of Re_s on the laminar side in Figure 3.17 (b) seem to be able to connect smoothly to those in Figure 3.17 (a). This is also true for the far variations on the turbulent sides, and thus the flow from one turbulent patch to the next can be reconstructed by placing the two conditionally sampled averages (LT and TL), side by side, while choosing an appropriate clipping time. For the reconstruction, we minimized the gaps of Re_s at the clipping time, keeping time durations on both sides of the interface equal, and we restricted the ratio of sum of the turbulent durations to the whole duration to be equal to the intermittency γ at $y = 0.5$. The inverse numbers of the optimized intervals for the reconstruction plotted in Figure 3.9 (a) and (b) are close to the average number of the turbulent patch passing, though they are slightly smaller and the peak position shifts more to the higher γ.

Figures 3.18 and 3.19 show the reconstructed variations of Re_s, the ensemble-averaged velocity, $\tilde{U}$, and the velocity fluctuation, $\tilde{u}$, for a duration longer than one period. For $\tilde{U}$ the time mean velocity, U, was subtracted. The connections are almost smooth at the clipping time not only in the Re_s variation but also in the averaged velocity and the fluctuation contour maps. This means that the reconstruction well captures the nature of the velocity field with passing a turbulent patch.

Figures 3.18 clearly indicates that variation of the local Re_s is drastic in the whole reconstructed duration. The total amplitude from the peak to the valley of Re_s is about 20% Re. The intersections of Re_s across the bulk Re are close to the clipping time, and the variation has approximate rotational symmetry with

respect to these intersections. This fact is consistent with the similarity of the conditionally averaged laminar and turbulence velocity profiles, in spite of the high amplitude of Re_s. Considering the wall-normal integration of the continuity equation, we deduced from the drastic variation of the Re_s that a large-scale field of the streamwise velocity accompanies that of the spanwise velocity. The direct numerical simulation by Fukudome et al.[7] shows that large-scale flow in the spanwise-streamwise plane circulates around the center of the inclined turbulent band. The drastic Re_s change strongly suggests the large structure similar to the flow with the turbulent band.

The laminar side velocity profile just after the turbulent patch constantly decreases. At the leading edge of the turbulent patch ($\Delta t = 0$), the velocity is low at the channel center, while the laminar side velocity close to the turbulent part trailing edge ($\Delta t = 19$) accelerates especially near the wall.

In contrast to the velocity profiles, the fluctuation distribution is almost constant in the laminar part, except for reduction at the channel center before the leading edge. The turbulent part has local intensification near the wall at the leading and trailing edges, and the fluctuation in the middle gradually increases. The highly fluctuated trailing edge is also investigated in a turbulent spot artificially generated in the channel flow. [40]

In the high Re case shown in Figure 3.19, an up-and-down variation of Re_s is observed in the turbulent part, in contrast to the monotonous increase of Re_s at $Re = 1650$. This undulation has a 30 d^*/U_b^* period and induces a higher-frequency component than that of the patch appearance. It is inferred that the departures of the very-low-frequency peak in the spectra maps (Figures 3.13 and 3.14) from the rate of the patch appearance in high-transitional Re can be attributed to this undulation.

Figure 3.20 shows Re dependence on these inclinations at the clipping time in the laminar and turbulent parts, $S = \frac{1}{Re}\frac{dRe_s}{dt}$. It is confirmed that the difference between the estimates from the switching conditions, LT or TL, is negligible. If the inclination is simply in proportion to the local Re difference, ΔRe_s, between the upstream and downstream interfaces, and in inverse proportion to the duration of the pure flow state, the slopes S_L or S_T would be represented by the following curves:

$$S_L = -\Delta Re_s \frac{N}{1-\gamma} \tag{3.12}$$

$$S_T = \Delta Re_s \frac{N}{\gamma}. \tag{3.13}$$

The inclinations following the curves illustrate that the velocity variation within each flow state is simply connecting the fringe edge velocities. This is also supported by the fact that the adopted values of the ΔRe_s, 0.16 and 0.18, for the laminar and turbulent inclinations, respectively, are very close to the difference between the laminar extrapolated values of Re_s/Re to the interface time in Figure 3.17 (a) and (b). We inferred that the discrepancy in the turbulence inclination at low Re is from the inconstant difference of the extrapolated values, in contrast to those for the laminar state. The reason for disagreement regarding the turbulent inclination with the curve in the higher Re is that there exists a turbulent part undulation, as described above.

3.6 Summary

The streamwise velocity averaged in the wall-normal direction in the reconstructed flow maps indicates the large-scale temporal variation. Considering that turbulent patches in the visualized transitional flow [9, 11] are slowly deforming with longer

temporal scale than their passing time, this temporal variation can be regarded as spatial change in the streamwise direction. As the velocity components averaged with respect to the wall-normal direction obey the two-dimensional continuous equation, their streamwise variation is concurrent with their spanwise variation. This indicates that there exist large flow structures in both the laminar and turbulent parts. The large-scale fluctuation is also confirmed in the velocity spectra maps as the peak at the very low frequency, and its frequency corresponds to an interval of the turbulent patch passing at the transitional Re. Around the upper marginal Re the peak frequency still increases with increasing Re, departing from the rate of turbulent patch appearance. It appears that the departure at high intermittency is due to the undulation observed in the turbulent part in Figure 3.19.

An explanation for the large-scale flow structure forming is illustrated in Figure 3.21 (a). As seen in Figure 3.18 (b), the ensemble-averaged velocity, $\tilde{U}$ near the wall increases in the turbulent patch, indicating high skin friction there. This seems to be due to high momentum transfer in the wall-normal direction. The high skin friction slows the patch down ('A' in the illustration). We infer that the decelerating patch hits an upstream laminar flow producing a high-pressure region (B) that makes the upstream laminar flow slow down. Because of continuity of the flow, this decelerating flow turns to the spanwise direction resulting slanted spanwise streams (C) around the downstream interface of the turbulent patch. Similar two dimensional flow around a turbulent band was observed in the direct numerical simulation,[7] and it is illustrated in Figure 3.21 (b). Slanted streams around the downstream interface of the turbulent band (D) and counter streams around the upstream interface (E) appear after subtracting the bulk velocity. We infer that the counter streams result keeping overall flow rate to be zero in both

streamwise and spanwise directions.

The scenario illustrated in Figure 3.21 (a) well explains the peak at the center of the channel in the wall-normal distribution of the low-pass-filtered fluctuation around $Re = 1500$, as seen in Figure 3.16. If a turbulent patch plays a role in a blockage, the pressure gradient in the streamwise direction uniformly acts over the whole channel width. Because of a viscous effect near the wall, the resultant velocity change is higher around the channel center. Therefore, the peak of the low-frequency fluctuation appears at the channel center. The moderate-frequency velocity fluctuation, whose scale is about ten times as large as the channel width, is also observed in the premultiplied spectra near the wall. It is obvious that this scale is larger than the scale of the turbulent disturbance and smaller than the scale for the patch passing. Considering the streamwise scale, the moderate-scale fluctuation seems to be caused by longitudinal vortical structures that were investigated upstream and downstream of a turbulent patch in the flow visualization.[9, 11] The near-wall peak in the wall-normal distribution of the band-pass fluctuation also suggests that this moderate-scale fluctuation is due to the vortical disturbance.

The large flow structures induce curvature of the streamline in the laminar part, due to the local pressure gradient in the streamwise and spanwise directions. We conjecture that generation mechanism of the longitudinal vortical structures is similar to instability in the three-dimensional boundary layer developing on a swept wing. The stream curvature due to the blockage of the turbulent patch makes the local shear flow unstable because of unbalance between the pressure gradient and the centrifugal force, and then this instability induces the longitudinal vortical structures. No matter what generates the moderate-scale structures, the enhancement of momentum transfer in the wall-normal direction makes the laminar part profile turbulent-like, and then the profile is very similar to the turbulent part

profile. The existence of the vortical structure is also supported by the fact that the shape factor drop is simultaneous with the increase of the band-pass-filtered fluctuation.

This momentum enhancement, however, leads to a contradiction that the deceleration of the laminar parts weakens the blockage effect of turbulent patches, which induces the pressure gradient that skews streamlines around the turbulent patches. The reduction of the blockage effect is insignificant in flows of very low intermittency around $Re = 1500$, because the momentum enhancement in the laminar part is restricted in the vicinity of turbulent patches, and then fresh laminar flow hits the turbulent patches, one after another. As a result, the low-frequency fluctuation caused by the local pressure gradient appears at the channel center, as seen in the low-pass-filtered map in Figure 3.16. The fact that the laminar part profile at $Re = 1520$ differs from that of the turbulent part, as shown in Figure 3.10, indicates that the laminar part is not filled up with disturbances inducing the wall-normal transfer of the momentum. With a decrease in the amount of the laminar parts with increasing Re, it becomes easy for the laminar part to be filled with the vortical structures. As seen in Figure 3.16, the band-pass-filtered fluctuation, which seems to be associable with the vortical structures, is predominant in the highly intermittent flow, $1600 < Re < 2000$. It is possible that the generation of the vortical structures by the streamwise skewness is delicately balanced with the blockage effect. This balance mechanism is also suggested by the fluctuation decline of the laminar part following the rapid increase up to $Re = 1500$. The fluctuation due to the blockage effect increases with increasing intermittency factor as far as the vortical structure spreads into all of the laminar parts. In high intermittency factor cases, the vortical structure reduces the blockage effect, and then it is slightly weakened adversely.

In conclusion, we propose definitions of two marginal Reynolds numbers of channel flow. The upper marginal Re is defined as the lowest Re for fully turbulent channel flow. The lower marginal Re is defined as the lowest Re for intermittent channel flow with laminar and turbulent parts. Since the large-scale flow structure enables local regions of higher Re, turbulence can partly generate or survive even when the bulk Re is lower than the limit for a sustainable turbulent flow, i.e., the upper marginal Re. The results of the streamwise energy decay and the intermittency factor dependence on the bulk Re indicate that the lower marginal Re is around 1400, though we observed turbulent patches lower than this value. For more precise determination of the lower marginal Re, a longer channel facility than the present one is needed.

As the spectral and conditional-average analyses indicated, the transitional channel flow has the large-scale flow structure with the turbulent patch appearance. To apply the concept, 'edge state', to the transitional channel flow, the analysis should take this scale into account. The fact that the large-scale structures are observable even in the conditionally sampled flow field suggests that they are robust and long-lasting. If some flow structure appears frequently in the transitional channel flow, it is great possibility that the edge-state captures its feature.

In the center spectra map of Figure 3.13, the peak of the large-scale disturbance continues from the transitional Re to the turbulent flow at $Re = 2660$ with little change of the peak frequency. In addition, the undulation of this scale is confirmed within the turbulent part just below the upper marginal Re. These results strongly suggest that the physical mechanism organizing the large-scale disturbance in the turbulent flow is the same in the transitional flow. The streamwise length scale of the disturbance equaling about 25 channel widths is very close to the superstructure in the fully developed turbulent channel[41] at about $Re = 140000$. The relation

between them is one of the interesting open questions about turbulent channel flow.

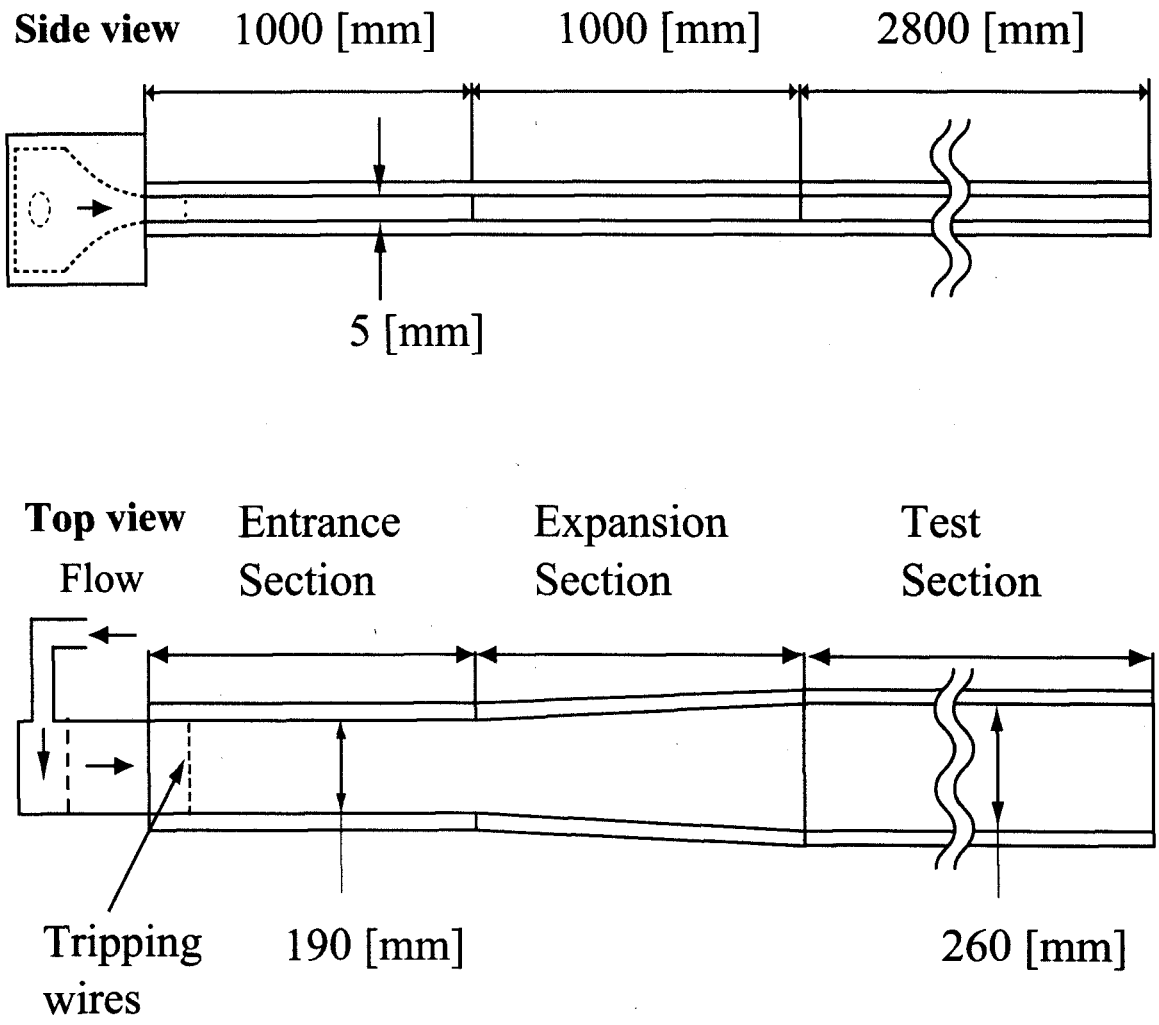

Figure 3.1: Air channel flow facility.

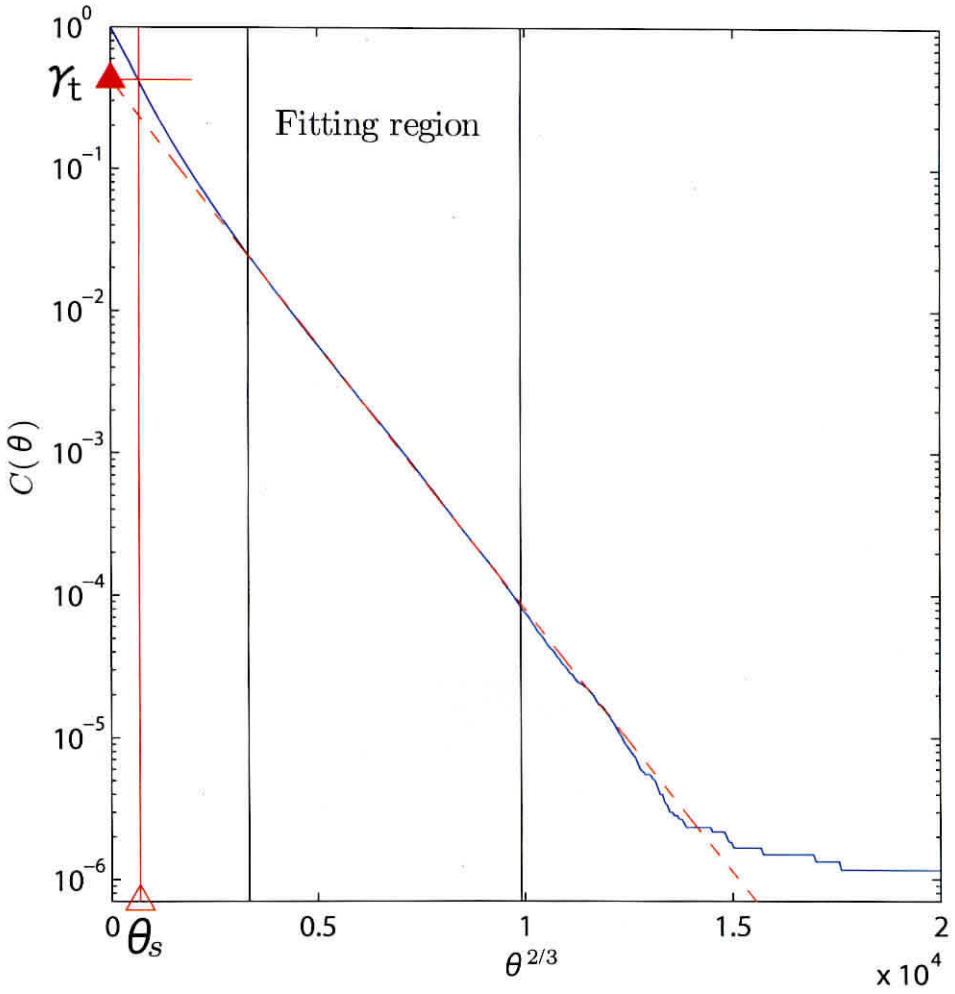

Figure 3.2: Single-slope method for the complementary cumulative distribution function $C(\theta)$. The dashed line is the fitting line. Solid and open triangles indicate a tentative intermittency factor γ_t and a threshold value θ_s, respectively.

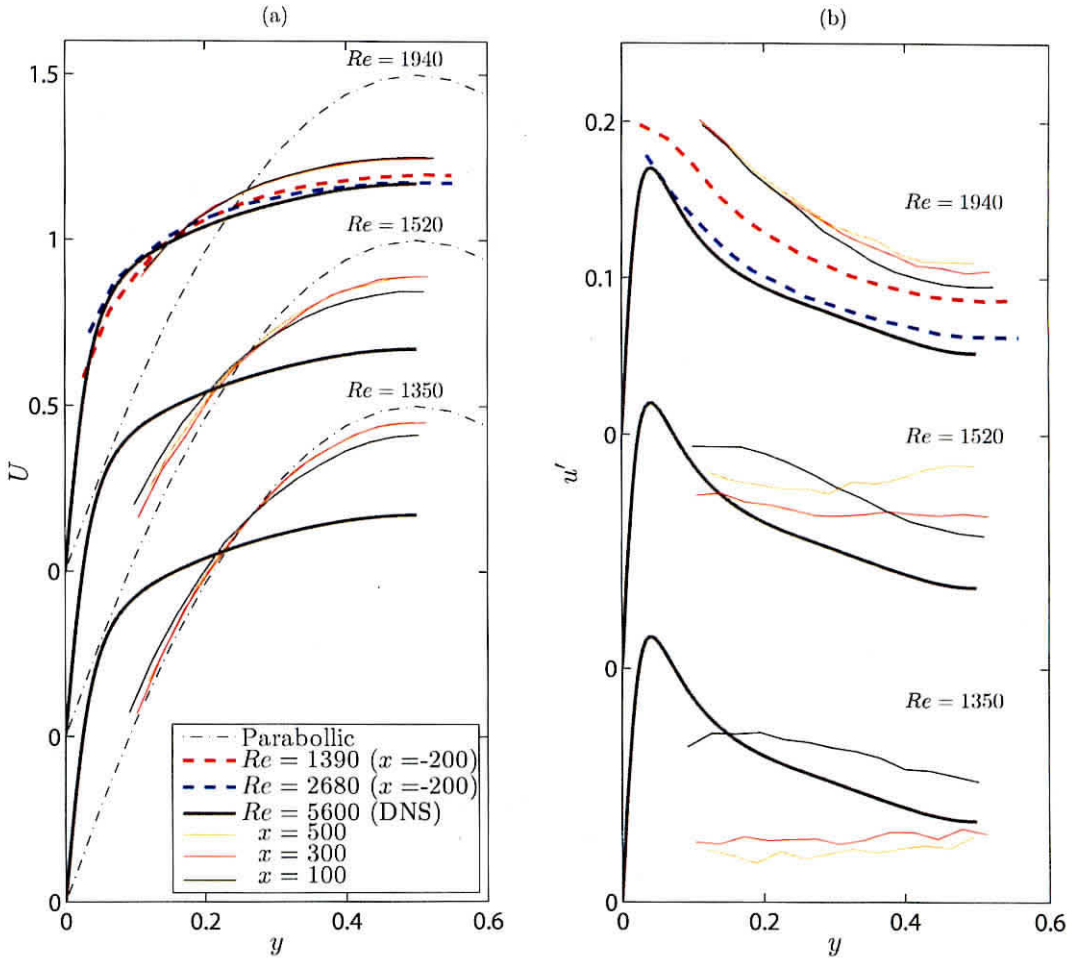

Figure 3.3: Streamwise variations of the mean velocity profiles and the distributions of the streamwise velocity fluctuation. (a) Mean velocity profiles. (b) Streamwise velocity fluctuation.

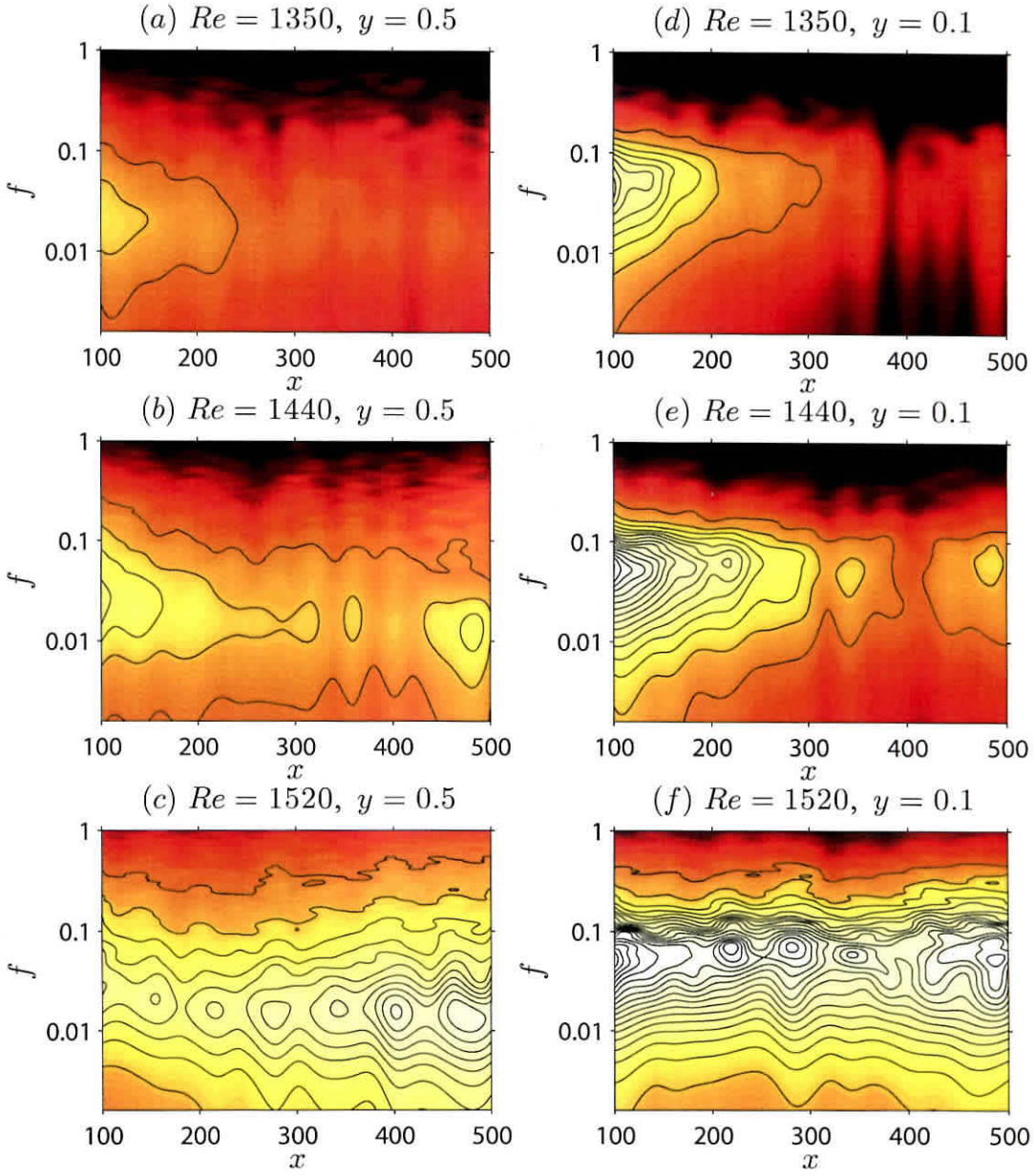

Figure 3.4: Streamwise variations of the velocity fluctuation energy spectra.

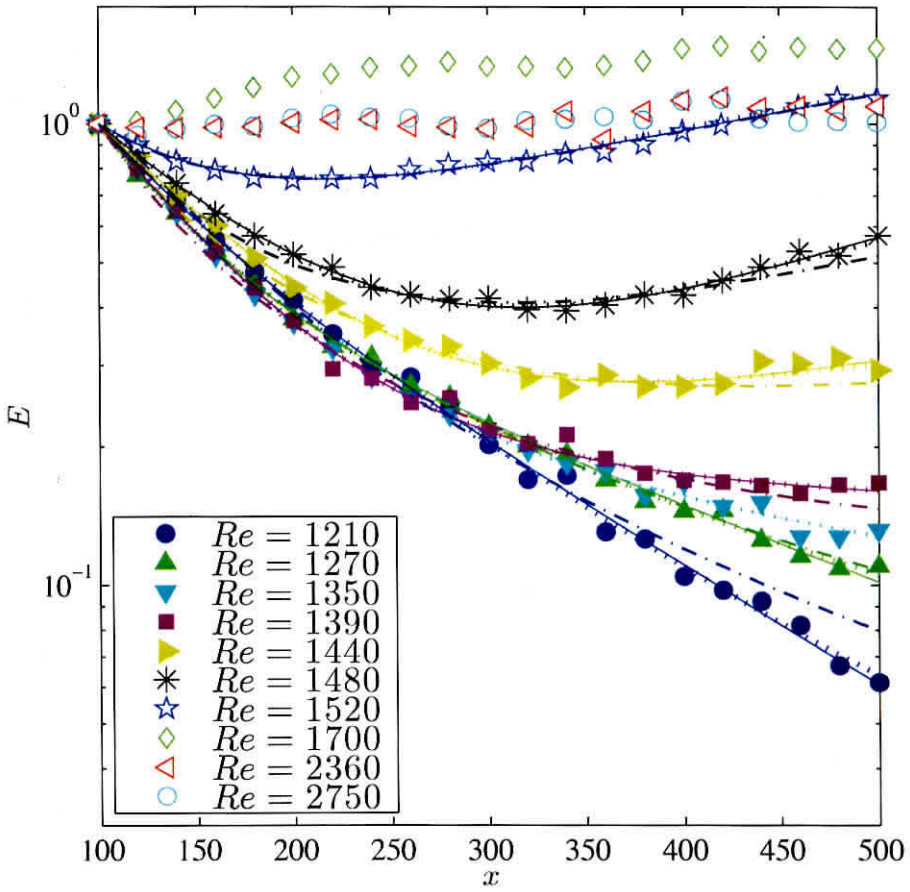

Figure 3.5: Streamwise variations of the velocity fluctuation energy. Solid, chain and dotted lines are fitting curves of Eqs. (3.5), (3.6) and (3.7), respectively.

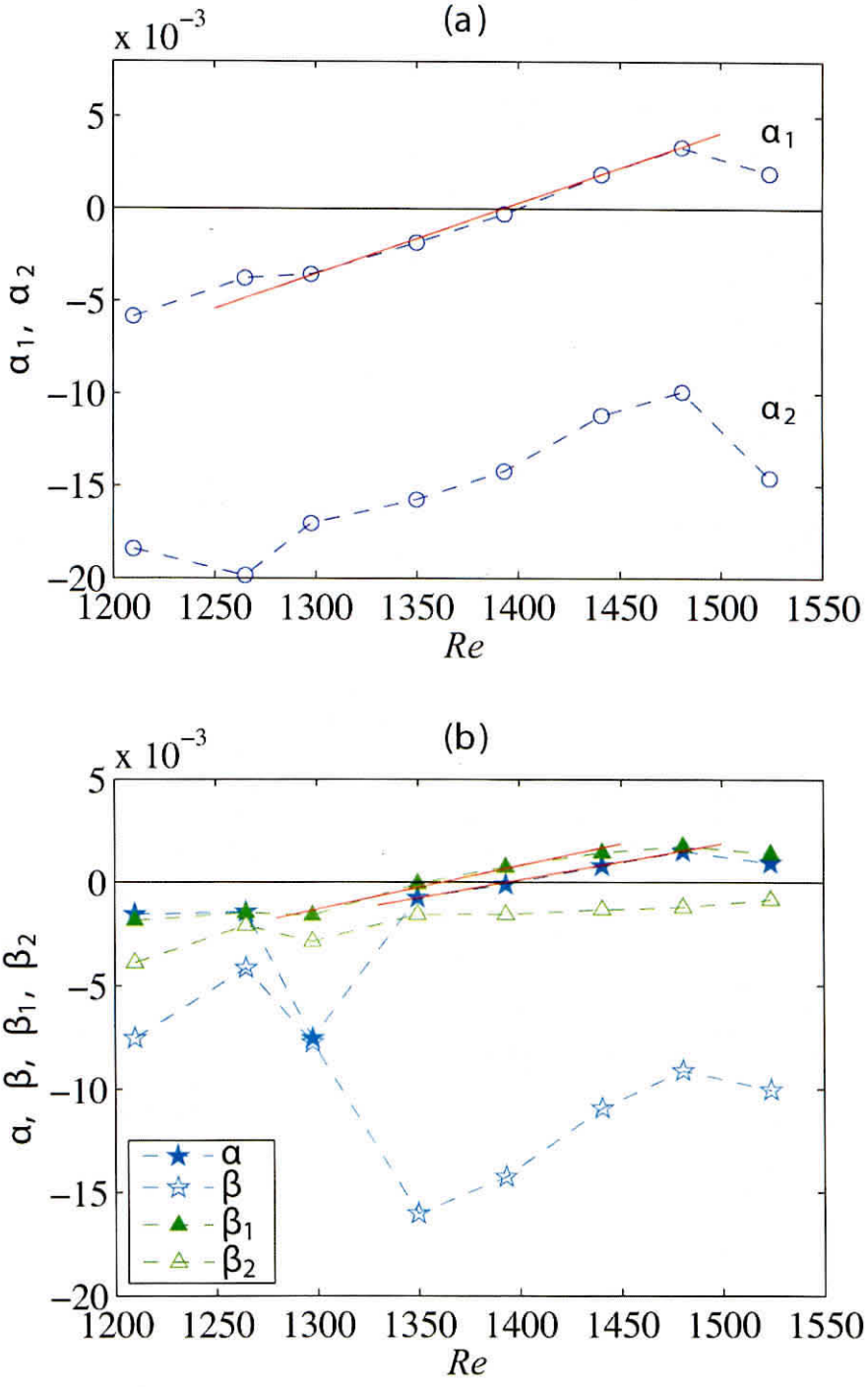

Figure 3.6: *Re* dependence on the growth rates and the exponent for the streamwise energy variation curves. Solid lines are the linear fitting.

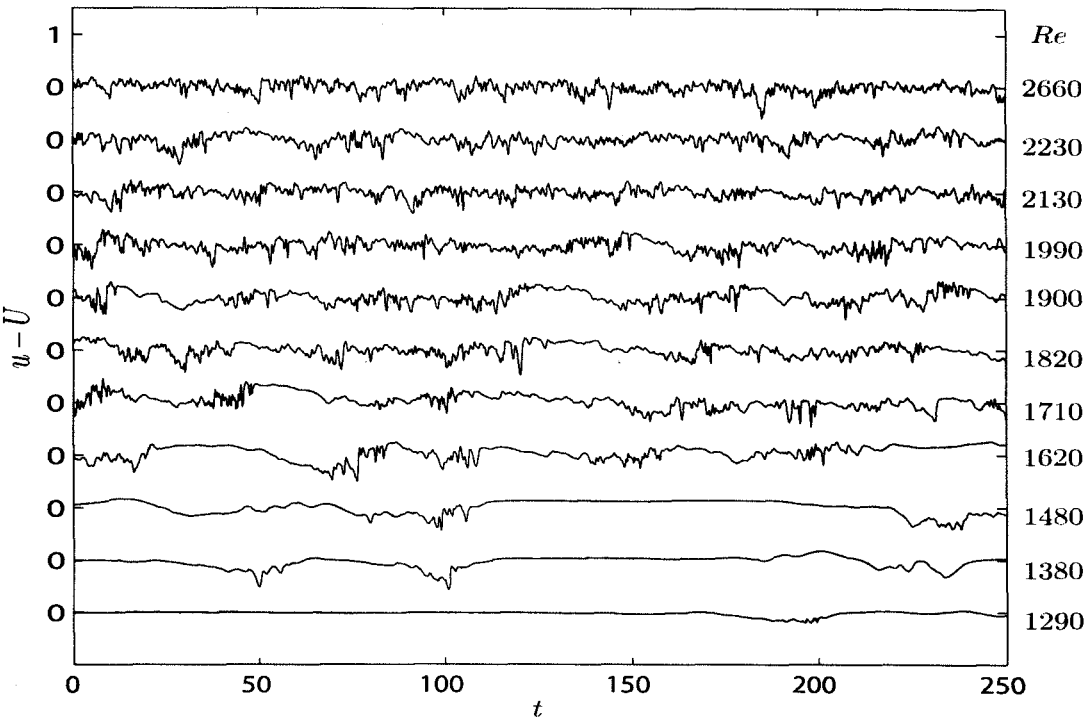

Figure 3.7: Time traces of the streamwise velocity at $y = 0.5$, $x = 500$.

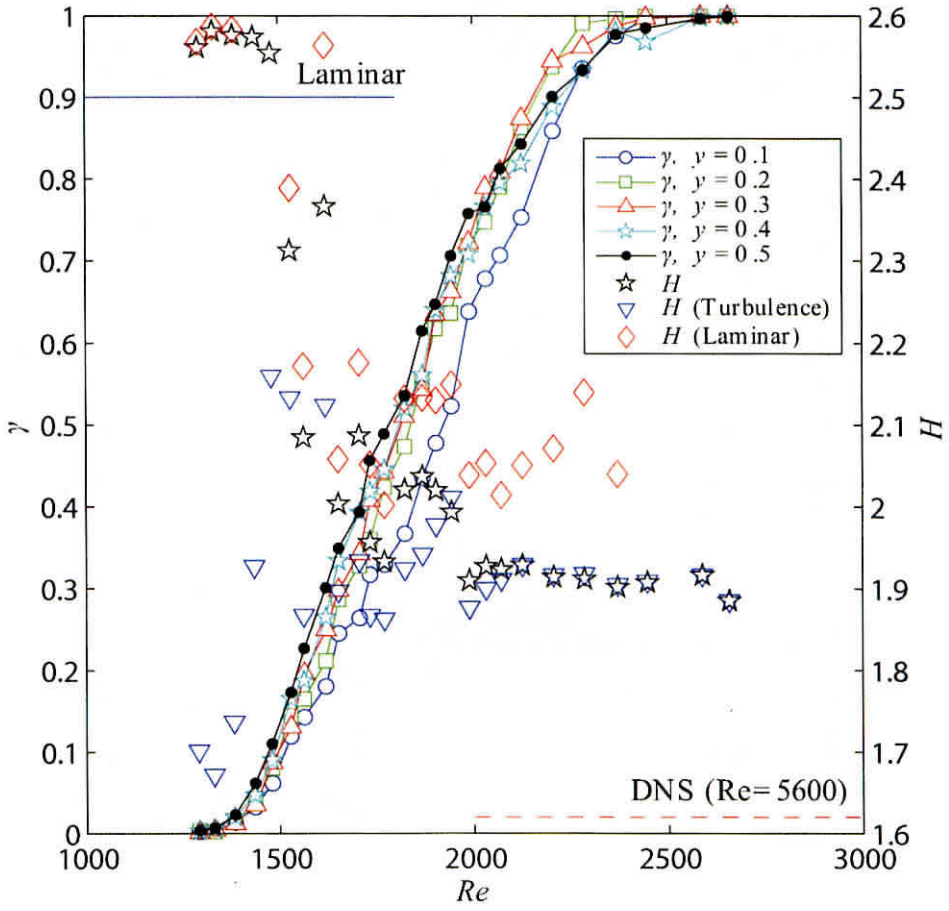

Figure 3.8: Intermittency factor γ and shape factor H as functions of Re. The horizontal solid line is the value of Poiseuille profile, and the dashed line is the turbulent channel at $Re = 5600$ (DNS).[12]

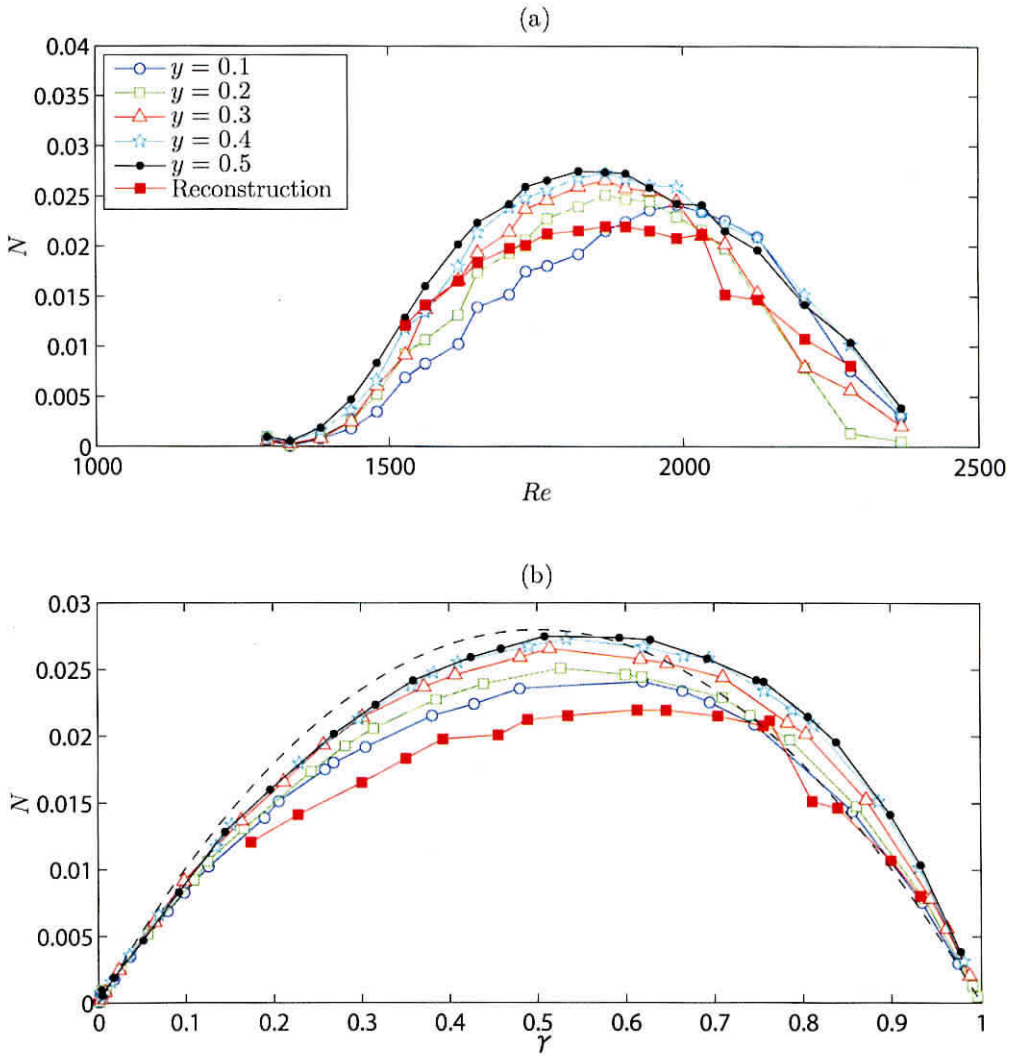

Figure 3.9: Number of turbulent patches. (a) N vs. Re. (b) N vs. γ. The dashed line is the parabolic distribution.

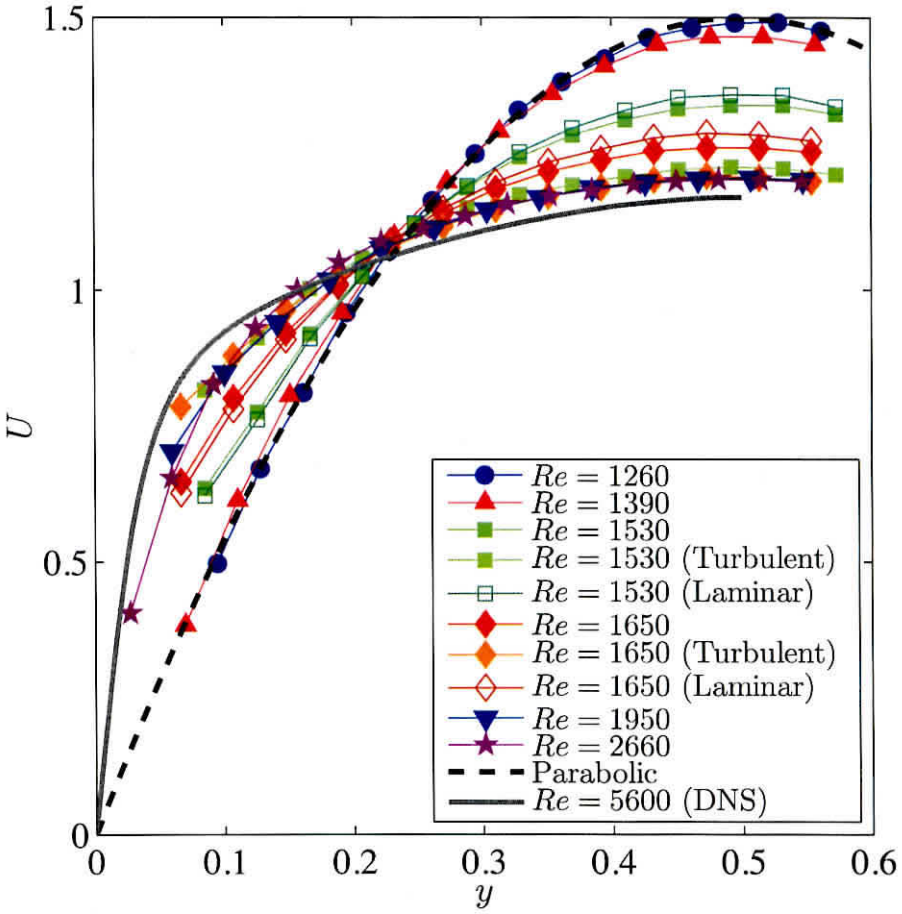

Figure 3.10: Mean velocity profiles. The DNS profile is from Kim et al.[12]

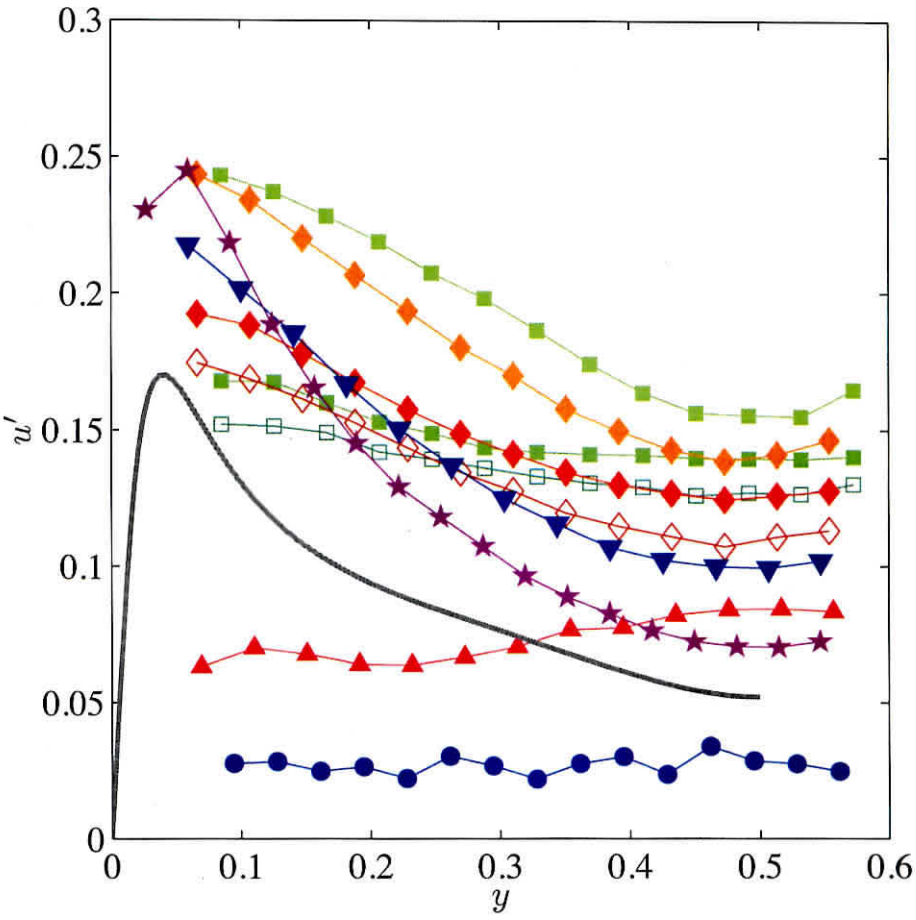

Figure 3.11: Velocity fluctuation distributions. The symbols are the same as in Figure 3.10.

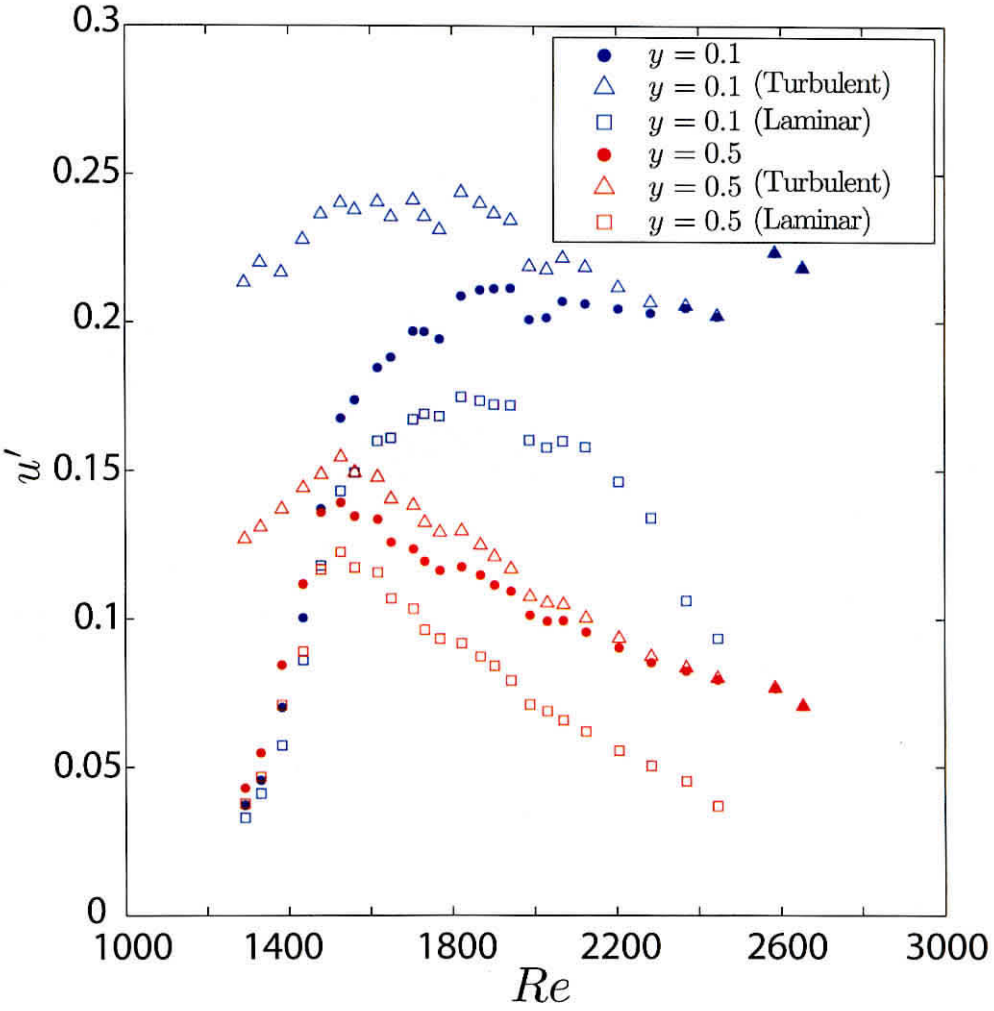

Figure 3.12: Re dependence of velocity fluctuations at the center, $y = 0.5$, and near the wall, $y = 0.1$.

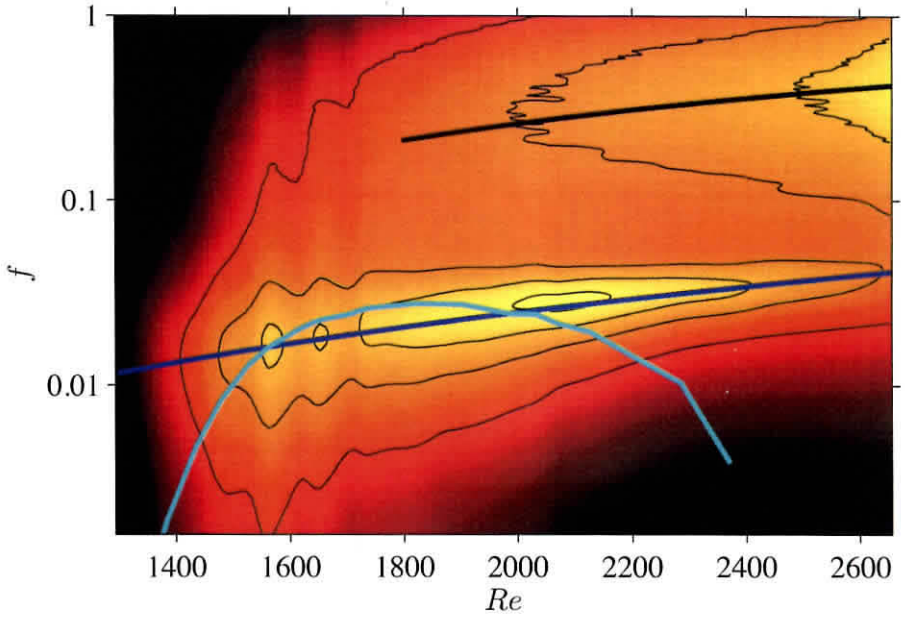

Figure 3.13: Contour map of the premultiplied energy spectra at $y = 0.5$.

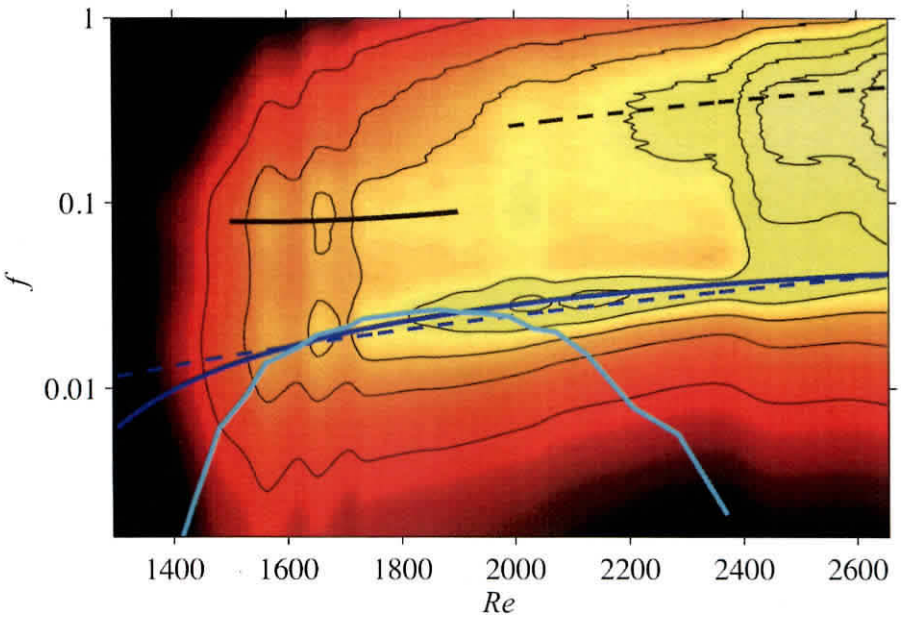

Figure 3.14: Contour map of the premultiplied energy spectra at $y = 0.3$. Dashed lines indicate the peak positions at $y = 0.5$. The contour space is the same as in Figure 3.13.

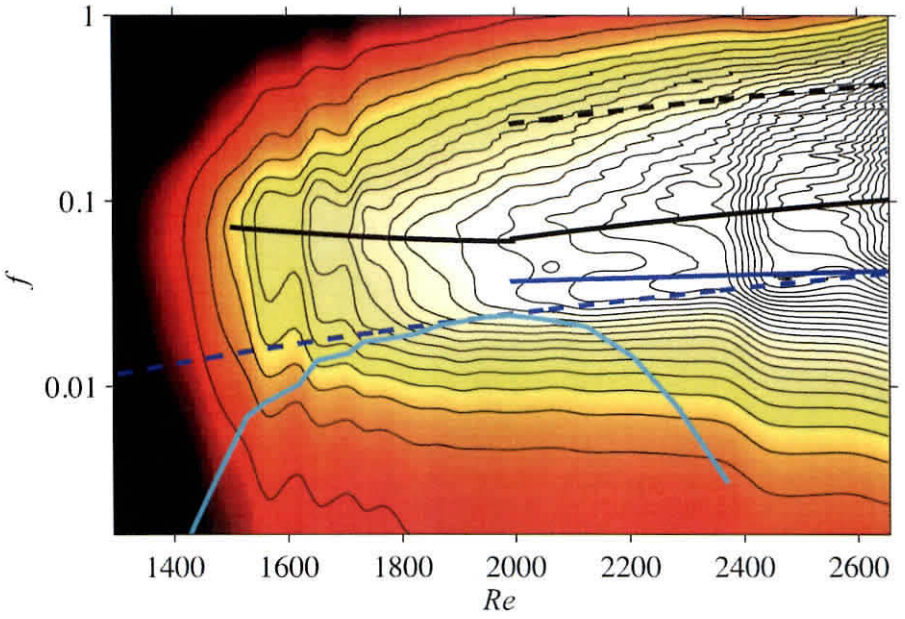

Figure 3.15: Contour map of the premultiplied energy spectra at near the wall at $y = 0.1$. Dashed lines indicate the peak positions at $y = 0.5$. The contour space is the same as in Figure 3.13.

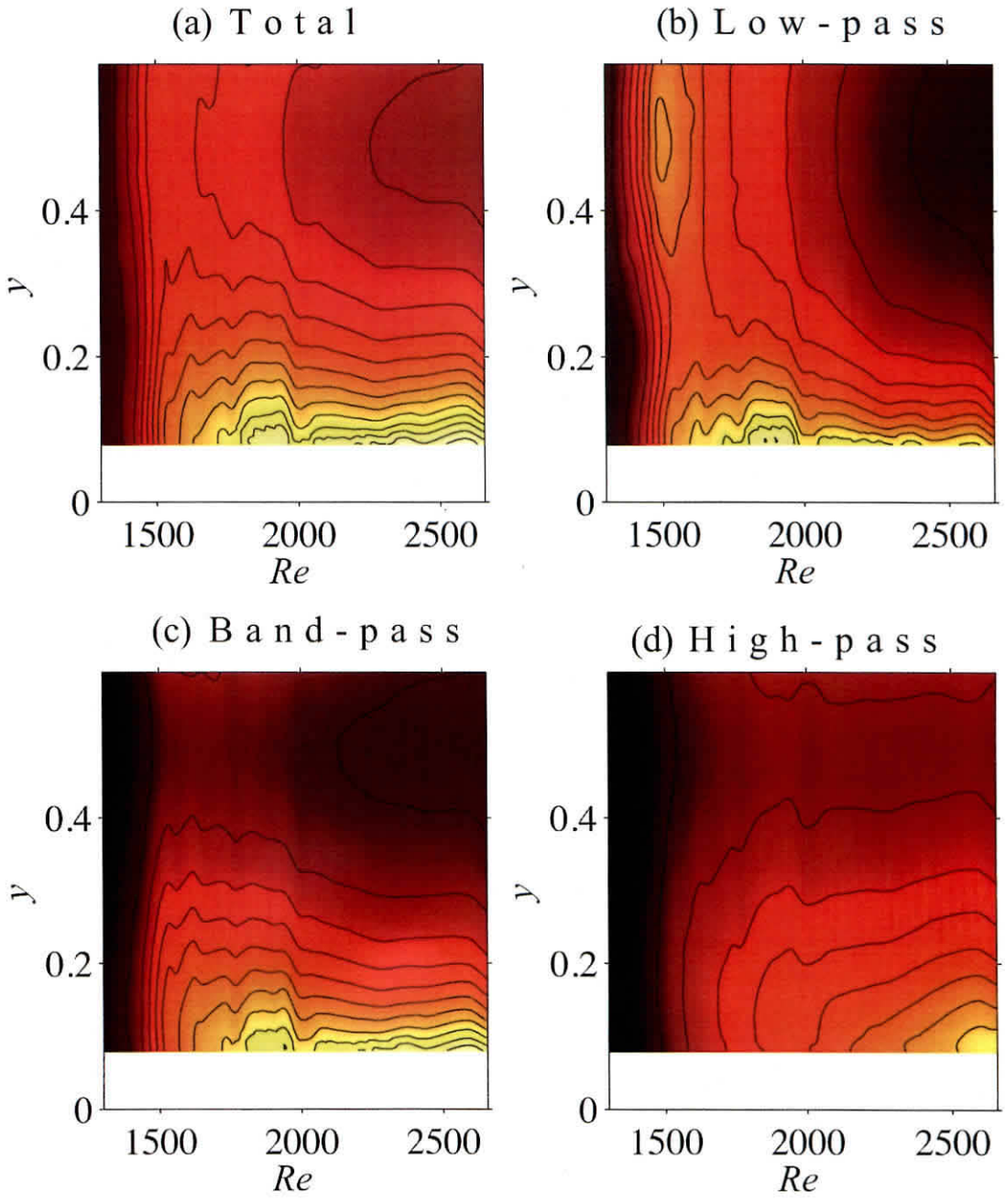

Figure 3.16: Distributions of energy of the streamwise velocity fluctuation in the $(Re - y)$ plane. Contour spacing is 0.4% for (a), 0.2% for (b), (c) and (d).

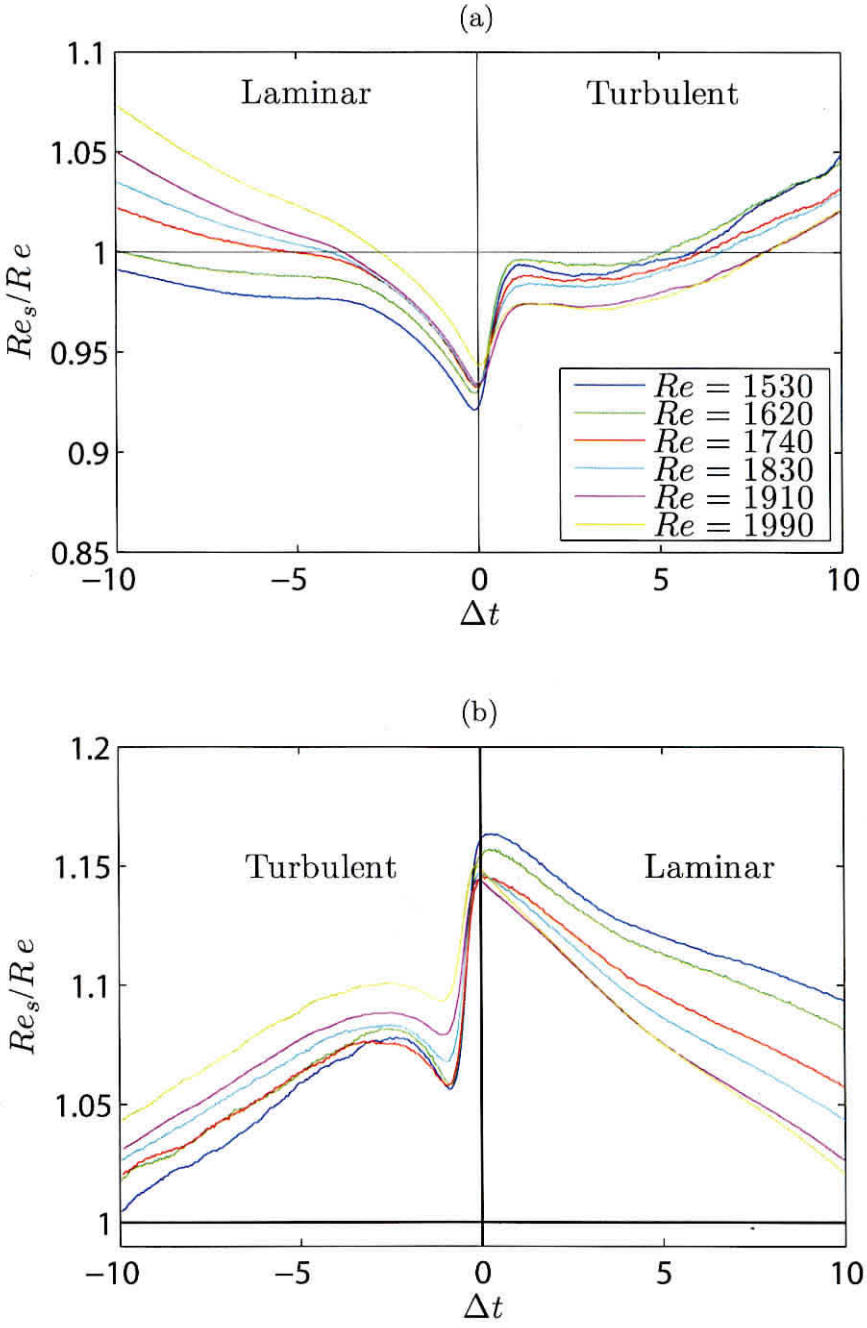

Figure 3.17: Conditional sampled time variations of Re_s/Re around interfaces between laminar and turbulent parts. (a) From a laminar part to a turbulent part (LT). (b) From a turbulent part to a laminar part (TL).

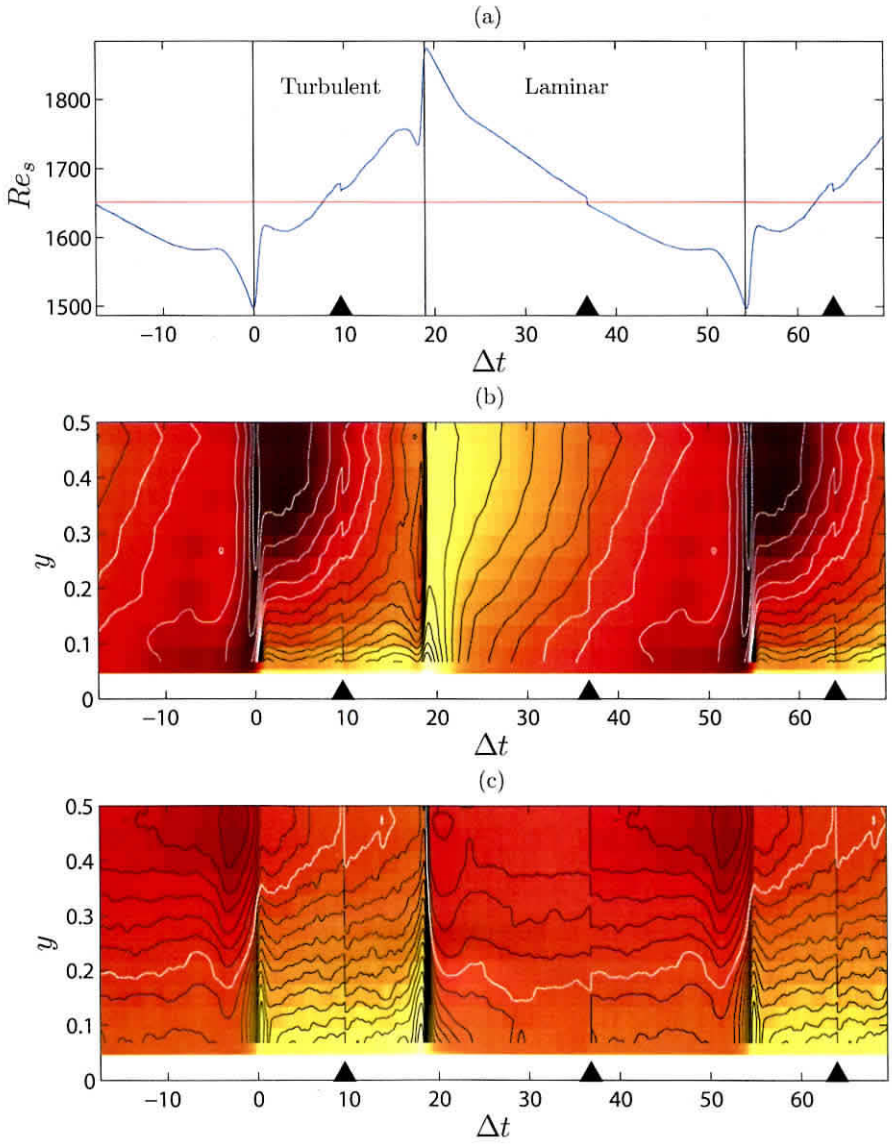

Figure 3.18: Space-time distributions of conditionally sampled results at $Re = 1650$. (a) Re_s. Solid vertical lines and solid triangles represent the interface time and the clipping time, respectively. Solid horizontal line indicates the bulk Re. (b) Contour plot of $\tilde{U} - U$. Higher value regions are lightly filled. The contour spacing is 2%, and negative contour lines are white. (c) Contour plot of $\tilde{u}$. The contour spacing is 1%, and white lines are for $\tilde{u} = 14\%$.

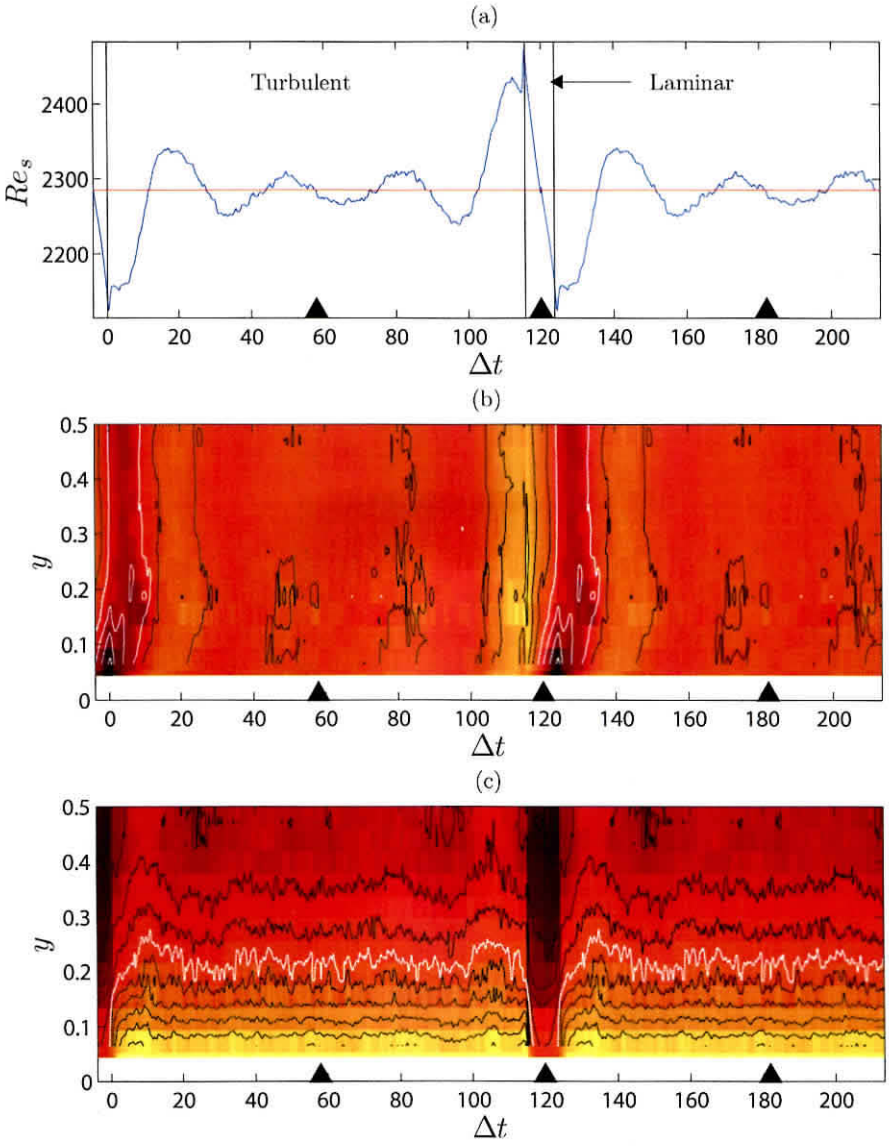

Figure 3.19: Space-time distributions of conditionally sampled results at $Re = 2290$. Representation is the same as in Figure 3.18.

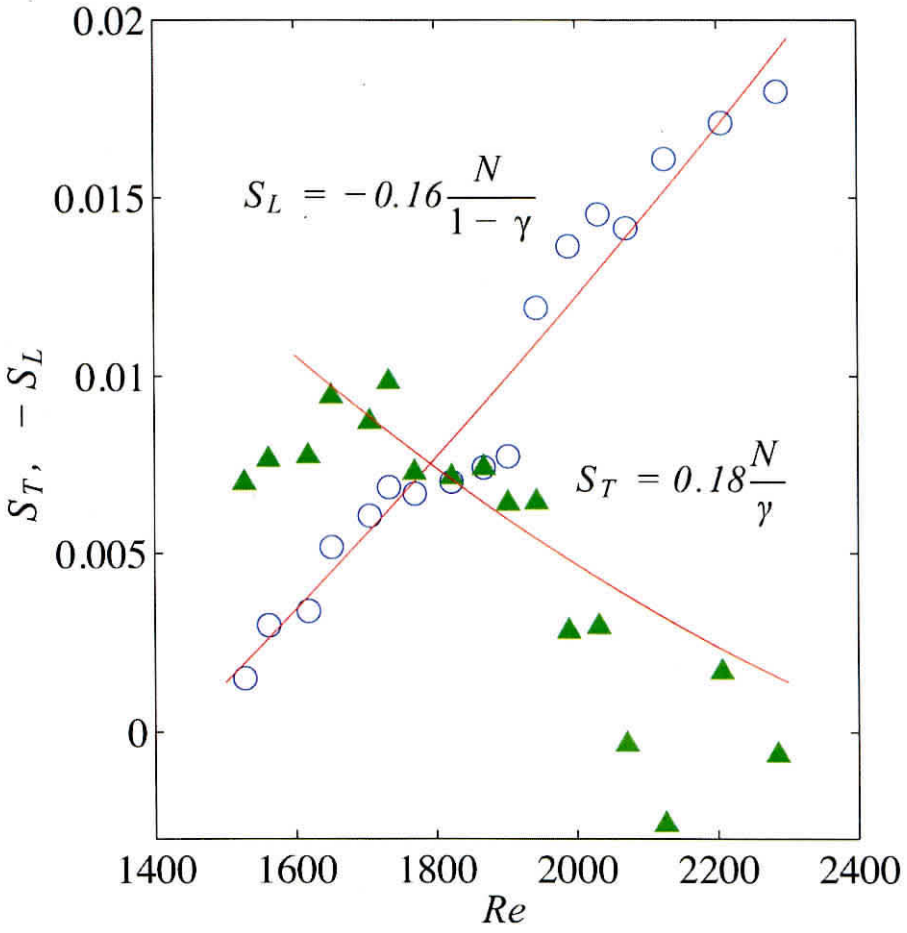

Figure 3.20: Inclination of Re_s at the clipping time. Circles, laminar part; triangles, turbulent part.

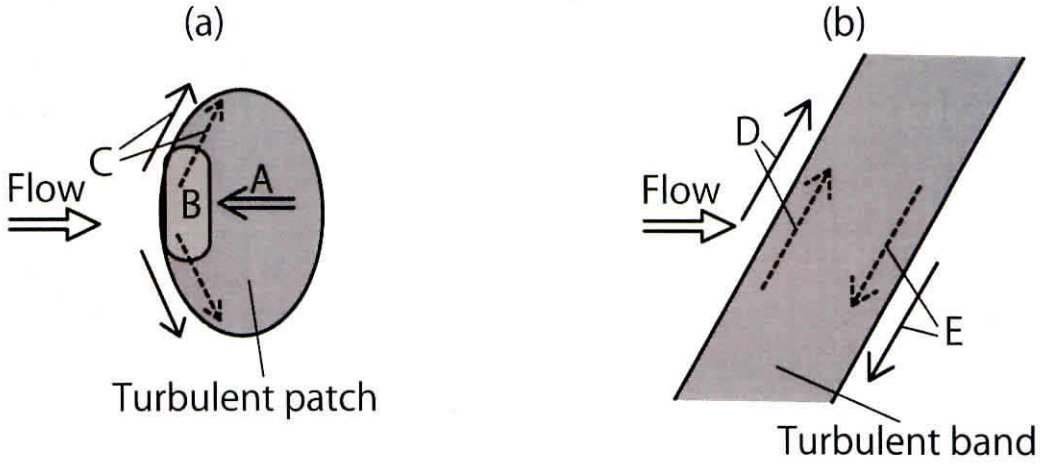

Figure 3.21: Illustration of intermittent channel flows. (a) turbulent patch. (b) turbulent band.

CHAPTER 4

Numerical simulations of relaminarizng and transitional channel flows

4.1 Preliminaries

In some range of Reynolds number, shear flows are in a transitional state between the laminar and turbulent regimes. In unstable shear flow, such as a boundary layer on a concave wall, unstable modes grow and the transition proceeds with energy propagation in the spectral space, while stable or neutrally stable shear flow such as a boundary layer on a convex wall undergoes intermittent transition in which disturbances distribute in the real space. Contrary to the streamwise-proceeding transition in a boundary layer, transitional channel flow between two flat plates can maintain in quasi-equilibrium of the disturbance energy as found in plane Couette flow, so it is more accessible to investigate into sustainability or growth mechanism of disturbances. Therefore, we performed direct numerical simulation (DNS) of the transitional channel flow that is realized in the reverse transition from turbulent to laminar flow with reducing Reynolds number.

The experiments and numerical simulations of transitional channel flow has been performed by many researchers. For the summary of their studies, see Seki et al. [42] As a theoretical approach to transitional shear flow, Kawahara and Kida[43] found the periodic motion in plane Couette turbulence and attempt to

relate it to flow statistics. To explain a puff or slug appearance in transitional pipe flow, a new concept, the edge state was proposed and it succeeded in describing the abrupt behavior of the transitional pipe flow.[24, 29, 30, 31] These theoretical approaches are expected to apply successively to the transitional channel flow.

Hot-wire measurements by the authors [42] determined the range of transitional Reynolds number and probed that there exist strong two-dimensional streams among and inside the turbulent patches, from the large fluctuation of the conditionally sampled velocity signals. The large flow structure was also supported by the pre-multiplied spectra of the streamwise velocity fluctuation. They also confirmed the turbulent-like profile in the laminar part of the transitional flow, indicating enhancement of streamwise momentum transfer in the wall-normal direction. We infer that this enhancement is caused by the streaky structures in the laminar parts observed in the flow visualization.[9, 11]

To investigate the two-dimensional streams and the streaky structures in detail, we carried out DNS with parametrically changing Reynolds number. After comparison with the hot-wire measurements for validation of the simulation, we propose generation mechanisms of the two-dimensional streams and the streaky structures.

4.2 Numerical method and conditions

A series of DNS has been performed between $Re = 1100$ and 3000, until 500 non-dimensional timesteps, $t = 500$, where the Reynolds number Re is defined by the bulk mean velocity, U_b, and the channel width, d, and all variables are normalized by U_b and d.

The DNS has been performed using the "channelflow" [44, 45] code that inte-

grates the incompressible Navier-Stokes equation using a spectral method based on the Fourier-Galerkin spatial discretization in the streamwise (x) and spanwise (z) directions, and Chebyshev-tau discretization in the wall-normal (y) direction. Time integration is performed using the third-order Runge-Kutta method. The 3/2 rule was applied for elimination of aliasing. The streamwise and spanwise dimentions of the computational box are 10π and 8π, respectively. The discrete points are 341, 65 and 170 in the streamwise, wall-normal and spanwise directions, respectively. Non-slip conditions are adopted at the wall-normal boundaries and periodic conditions are for the streamwise and spanwise boundaries. The streamwise pressure gradient is imposed to keep the mass flux constant. For more details about the method of DNS, see Refs. [44, 45]

4.3 Result and Discussion

Comparison of statistical results with the experiments [42] is shown in the section below, both for validation of the simulation and overview of the transitional channel flow.

For investigation of the transitional or laminarizing flows, Re dropped from the initial Reynolds number Re_i to the target Reynolds number Re ranging between 1100 and 3000. The fully developed flow field at $Re_i = 2400$ was taken as initial condition at the beginning. All runs of DNS were monitored with the total energy variation E in time as shown in Figure 4.1. The total energy was obtained by integration of the square of the streamwise velocity fluctuation u_{rms}^2 in the whole domain, and it was normalized by that at the Re dropping time, $t = 0$.

For $Re \geq 1600$, E recovers to an equilibrium value within 150 non-dimensional timesteps after a decrease to the minimum. At $Re = 1400$, E monotonically

decreases for the initial condition $Re_i = 2400$ indicating that flow is laminarizing. We also observed relaminarization at $Re = 1500$, which was doubted because the value is too high comparing with the experiments. Then we recognized that below $Re = 1500$ the flow strongly depends on the initial condition, and we noticed tendency that laminarization occurs with large difference of Reynolds numbers, $Re_i - Re$, though there an exception of recovering was observed at $Re = 1500$ for $Re_i = 2600$. This strong dependence of the initial condition is not surprising since the flow is subcritical. For simulation of the transitional flows, we reduced Re_i to 2200 for the target Reynolds number $1450 \leq Re \leq 1500$ and $Re_i = 1800$ for $1350 \leq Re \leq 1400$. In the present runs non-laminarizing flow was simulated for $Re \geq 1350$. For comparison, the experimental results are also plotted with space-time conversion $t = (x_{exp} - 100)/U_b$, where x_{exp} is the non-dimensional distance from the inlet of the test section.

Except for the monotonic decay at $Re = 1300$, 1400 and 1500 for $Re_i = 2400$ in Figure 4.1, E recovers to the same level as the initial energy. It is noticed that the energy at $Re = 1530$ recovers after reading a minimum of 40%. Slow undulations of E after the recovering are observed as well as the experimental result at $Re = 1700$. In the laminarizing cases, the lower Re, the faster the monotonic energy decays.

The energy variations in the recovering cases also depend on the initial conditions as seen at $Re = 1500$. The energy increase in the recovery is quicker in the simulation than in the experiment. We infer that this is due to the limited computational box in the simulations. Even for the slowest recovery at $Re = 1500$ for $Re_i = 2200$, E reaches the constant value, indicating that the flow is in quasi-equilibrium states, within 300 non-dimensional timesteps. Therefore, we used results in $300 \leq t \leq 500$ for the statistical averages.

In Figure 4.2 the intermittency factor, γ, is compared with hot-wire measure-

ments. γ was estimated by the single-slope method that was successfully applied for the hot-wire signals [42]. For DNS data, we take wall-normal integration of the spacial second derivative of the streamwise velocity u,

$$D = \int_0^1 \left| \frac{\partial^2 u}{\partial x^2} \right| dy, \tag{4.1}$$

as a detector function instead of the temporal second derivative for the hot-wire signals. This detector smoothly distributes in x-z plane, so that filling and discarding process, which was used for the hot-wire signals to remove in unnaturally short laminar or turbulent durations, is unnecessary in order to divide the flow into laminar or turbulent parts. We confirmed that the wall-normal integration does not affect γ.

γ is linearly increasing with Re from $Re = 1500$ and reaches unity at $Re = 2200$. The simulation result is in very good agreement with the experimental results at $y = 0.3$ and 0.5 in the range of $1650 \leq Re \leq 2100$. Seki and Matsubara[42] proposed the characteristic Reynolds numbers for the transitional channel flow. One is the lower marginal Re_p that is defined as the lowest Re for intermittent channel flow with laminar and turbulent parts, and the other is the higher marginal Re_f defined as the lowest Re for fully turbulent flow. The DNS result in Figure 4.2 indicates $Re_p \leq 1350$ and $Re_f = 2200$. The simulation more quickly reaches the fully turbulent state of $\gamma = 1$ than the experiments. Re_f seems to be underestimated because the transitional flow with small ratio of laminar part cannot be simulated with the limited computational box. γ for $Re \leq 1500$ is higher than the experiment and is slightly scattered. In the experiments, the energy, E, for $1440 \leq Re \leq 1480$ still increases at the measurement position $x_{exp} = 500$, so γ would increases downstream.

Figure 4.3 shows the relation between Re and the skin friction coefficient, C_f.

Laminarizing cases for $Re < 1350$ with $Re_i = 2400$ are also plotted. In the range $1350 \leq Re \leq 1500$, two values in the laminar and transition states are plotted. At $Re = 3000$, C_f of the DNS is very close to the experimental result obtained by Patel and Head.[3] For $2200 \leq Re \leq 3000$, C_f follows the -1/4 slope as well as the turbulent pipe flow resistance for low Reynolds number. The deviation from the slope increases with decreasing Re though C_f at $Re = 1350$ still keeps a level that is about 30% higher than the laminar value. The length of the channel that was used by Patel and Head was 288 channel widths, and they introduced initial disturbances upstream in the channel in which Re is the same as the measurement position. These experimental conditions might cause undeveloped flow at their measurement position.

We divided the flow into laminar and turbulent parts by a threshold for the detector function. The threshold was decided by the single slope method. For convenience, we call the non-turbulent part 'laminar' though it sometimes contains strong disturbances. The turbulent C_f follows the $-1/4$ slope with decreasing Re and deviates to slightly higher values. It is noted that the laminar C_f is much higher than that of the parabolic profile flow, though there exists difference between the laminar and turbulent C_f of more than 5% in the transitional range of $1350 \leq Re \leq 2150$.

The shape factor, H, shown in Figure 4.4. H is defined as

$$H = \frac{U_c \int_0^1 (U_c - U)dy}{\int_0^1 U(U_c - U)dy}, \tag{4.2}$$

where U is the time-averaged velocity and U_c is the center mean velocity. H is around 2.2 at $Re = 1350$ and then gradually decreases with increasing Re and approaches to the DNS value by Kim et al.[12] at $Re = 5600$. Though the

simulation does not capture the sudden drop in the experimental result around $Re = 1500$, the gradual decrease quantitively agrees with the experiment. H for the laminar flow is slightly larger than the value for the whole flow. The low value of the turbulent H indicates that the velocity profile of the turbulent part keeps the standard turbulent profile even for low Re.

Figure 4.5 shows the mean velocity profiles and distributions of the velocity fluctuations. The profiles at $Re = 1700$ and 2650 are in good agreement with the experimental profiles. The profiles for $Re \geq 2650$ capture the characteristics of the turbulent profile with acceleration near the wall and deceleration around the channel center, as seen when compare to DNS result of the fully developed turbulent flow at $Re = 5600$.[12] The profile at $Re = 1350$ indicates a tendency of the turbulent characteristics, comparing with the experimental profile that is of the laminarizing flow. It is noted that there is no difference between the mean profiles of the laminar parts and the whole in the transitional range of Re and the mean profiles of the turbulent parts are also the same except at $Re = 1350$. The correspondence between profiles of laminar and turbulent parts was also found in the simulation by Fukudome et al.[7]

As seen in Figure 4.5 (b), (c) and (d) the velocity fluctuations are more drastically changed with Re. For turbulent range of $Re \geq 2650$ the streamwise velocity fluctuation u_{rms} has a peak around $y = 0.05$. In the range of transitional Re, the peak values of the laminar part and the whole increase with increasing Re while in the turbulent profiles the peak value decreases. Comparing the u_{rms} distributions between the laminar and turbulent parts, the turbulent distributions are always larger than the laminar one. In both parts of the transitional flow, u_{rms} at the channel center is higher than that in the fully developed turbulent flow. The u_{rms} distribution of the DNS at $Re = 1700$ is similar to the experimental distribution

at $Re = 1710$ though the u_{rms} of the DNS is slightly lower. u_{rms} of the DNS at $Re = 2650$ is also lower especially near the wall. Because of the relaminarization at $Re = 1330$ in the experiment, the u_{rms} distribution is flat and much lower than the DNS.

The transitional flow has the characteristic that the wall-normal fluctuation v_{rms} shown in Figure 4.5 (c) rises around the channel center regardless of the flow state, laminar or turbulent, resulting in the plateau distribution. As shown in Figure 4.5 (d), this characteristic is enhanced in the distributions of the spanwise fluctuation w_{rms} of the whole and the laminar part, where the distributions of the laminar part have a peak at the channel center in the transitional flow. The distributions of fluctuations of the fully turbulent flow for $Re \geq 2200$ are very similar to the DNS result by Kim.[12]

The dependence of the u_{rms} on Re compared with the experiments is shown in Figure ??. The value of the whole at $y = 0.1$ increases with Re in the transitional Re range and gradually decreases for $Re \geq 2050$. In the experiment the tendency of gradual decrease is also observed in $1800 \lesssim Re \lesssim 2400$. Though the fluctuation of the turbulent part is lower than the experimental one, the DNS captures the Re dependence in the experiment in terms of the gradually decrease. The fluctuation of the laminar part are in agreement with the experimental result for $1500 < Re < 2000$. The DNS results at $y = 0.5$ indicate the clear peaks at $Re = 1500$ regardless of the flow state, though the increase before the peaks is modest in the DNS.

Figure 4.7 shows the peak values u_p, v_p and w_p in the wall-normal distribution of the velocity fluctuations u_{rms}, v_{rms} and w_{rms}, respectively. In the transition range of Re, u_p and v_p increases with Re while w_p fluctuates. All peak values of the turbulent parts decrease in the transition range and then increase in the turbulent range. It is worthy to note that the peak values in the turbulent range

of Re continue to increase, in contrast to the high Reynolds number turbulent boundary layer.

To summarize the comparisons between the present DNS and the experiment, the statistics are consistent, though the velocity fluctuations are lower in the DNS. The statistical results also suggest that in the laminar part of the transitional flow there exist large disturbances that increase the skin friction and the velocity fluctuation. The disturbances in the laminar parts are discussed below.

Before commenting on a snapshot of the velocity field, the phase velocity of the patches and the bulk velocities of laminar and turbulent parts will be discussed. The patch phase velocity U_p was estimated from the maximum correlations of the detector function D in the x-t plane. As seen in Figure 4.8, the mean velocities of laminar parts, U_L, and turbulent parts, U_T, are almost unity independent of Re, indicating they are the same as the whole bulk velocity U_b. The patch velocity is decreasing slightly with increasing Re in the transitional range. Fukudome et al. [7] also observed that the mean velocities of the laminar and turbulent parts are the same, and that a phase velocity of the slanted turbulent stripe is $1.02U_b$ close to the bulk velocity. The phase velocity for the turbulent range of Re is roughly constant though this value is not the patch velocity anymore since the flow is fully turbulent. The estimation of the phase velocity may relate to the large structures embedded in the turbulent channel flow.

Figure 4.9 shows a snapshot of the flow field in the whole computational box at $Re = 1600$. There exist two slanted turbulent patches with velocity fluctuations. Tsukahara et al.[46] observed slanted turbulent stripes in their large computational box. From observation of the time sequences, the pattern of the turbulent patches dynamically varies and any steady pattern never appears in the present simulations. Though this is contrary to the quasi-steady stripe pattern of the turbulent

part observed by Fukudome et al.[7], the temporal change of turbulent patch pattern was also confirmed in the flow visualization.[9, 11] The pair of streaks with alternating v in the z direction are seen upstream of the leading edges of the patches around $(x, y) = (10, 7)$ and $(25, 23)$. The scale of the patch is about $20d$ in the streamwise direction and $5d$ in the spanwise direction. The large-scale streams are observed both along the upstream and downstream edges of the patches, and the streamwise velocity in the laminar region decelerates downstream of the patch edges and accelerates upstream the edges.

This streamwise velocity change is clearly observed in the integrated streamwise velocity in the wall-normal direction, Re_s,

$$Re_s = \int_0^1 u \, dy, \tag{4.3}$$

as shown in Figure 4.10. In the direction of the flow, Re_s increases in the laminar part and decrease in the turbulent part. This supports that the conditional sampling of the hot-wire signals well captures an instantaneous flow field between two patches.[42] The amplitude of Re_s in the DNS is 40% that is comparable to 25% amplitude in the conditional sampling.

Figure 4.11 shows a y-z cross section of the instantaneous flow field shown in Figure 4.9. The vortices are alternatively located from $z = 4$ to 11 with the low streamwise velocity regions at the upward stream from the wall to the channel center suggesting the lift-up effect. These low and high velocity regions elongates to a length of about $10d$, as seen in Figure 4.9. They has an asymmetry in that the downward streams skew toward the positive z direction, the contrary is true for the direction of the upward stream. The spanwise size of the vortices is $1.2d$ and the wall-normal size exceeds half the channel width. In contrast to the longitudinal vortices, the turbulent vortices are randomly positioned inside the turbulent

patches.

To reveal the generation mechanism of the large-scale velocity undulation between turbulent patches as seen in Figure 4.10 and the conditional sampling,[42] the flow field integrated in the wall-normal direction is investigated in detail. Figure 4.12 (a) shows distributions of the detector function D and the integrated static pressure $\bar{p}$. Comparing to the x-z plane snapshot shown in Figure 4.9, it is confirmed that D well captures the turbulent regions. The high pressure regions are distributed around the downstream edges of the patches. The relative streamlines shown in Figure 4.12 (b) circulate in the laminal regions between the patches and inside the patches. These circulating streams were also confirmed in the flow with the slanted turbulent stripe in the DNS by Fukudome et al.[7] The absolute streamlines in Figure 4.12 (c), are obtained by adding $U_b z$ to the relative stream function. They skew as they avoid hitting the turbulent patches that play the role of blockage due to the higher skin friction than their surroundings.

As a result of the skewing there exist areas of high curvature of the streamlines in the laminar region as seen in Figure 4.12 (d). The curvature is estimated from $\partial\bar{w}/\partial x$, where $\bar{w}$ is the integrated spanwise velocity. It is obvious that emergence of the elongated vortex structures, which are clearly detected by the integrated wall-normal velocity $\bar{v}$, well correlates with the high curvature areas. This strongly suggests that the vortex structures grow due to a cross-flow instability such as three-dimensional boundary layer on a swept wing. It is noted in Figure 4.12 (c) that the areas of the vortex structure has high skin friction that causes greater C_f in the transitional channel flow than the parabolic profile value.

4.4 Summary

The intermittency factor and the mean velocity profile of the transitional channel flow are in good agreement with experimental measurements except at low Re of the transitional range. The detailed analysis with the wall-normal integration indicates that blockage effect of the turbulent patches induces a two-dimensional flow of large-scale around and inside the turbulent patches. Appearance of the streaky structures well correlates to the streamwise curvature of the streamline skewed by the blockage, suggesting that a cross-flow instability induces them. The streaky structures locally enhance the wall normal momentum transfer that causes high total skin friction in the transitional flow even at a low intermittency factor.

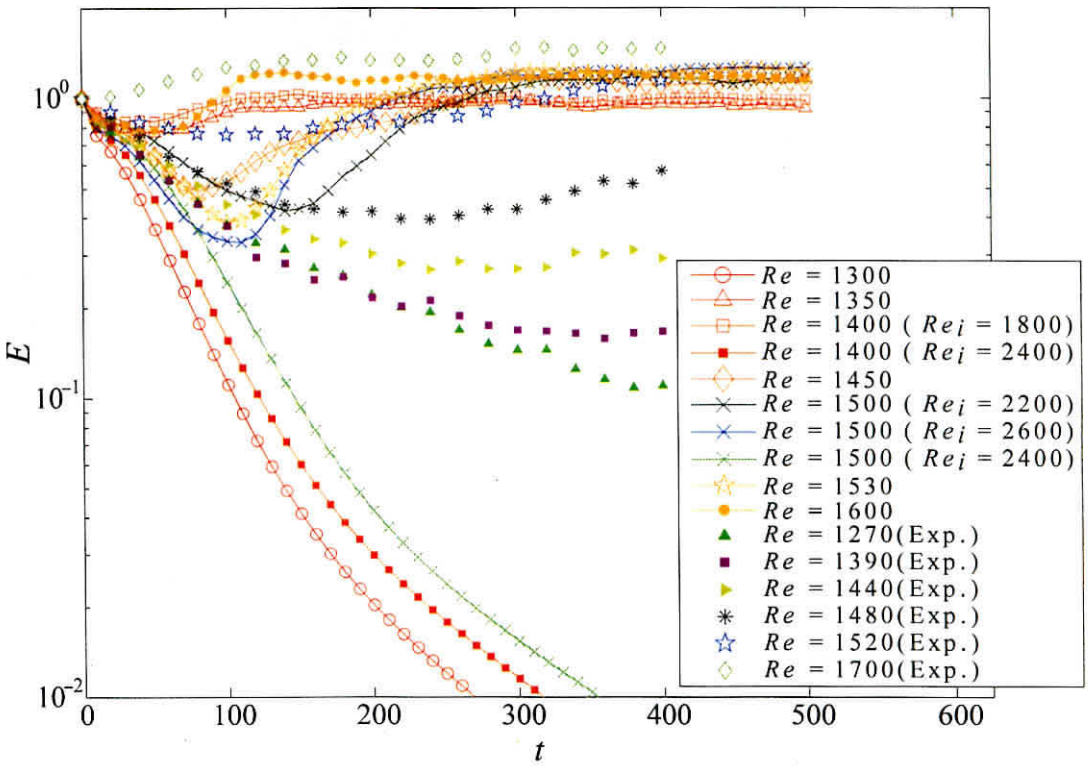

Figure 4.1: Time variation of the velocity fluctuation energy. In experimental data, the horizontal axis was rescaled to compare the presnt results.

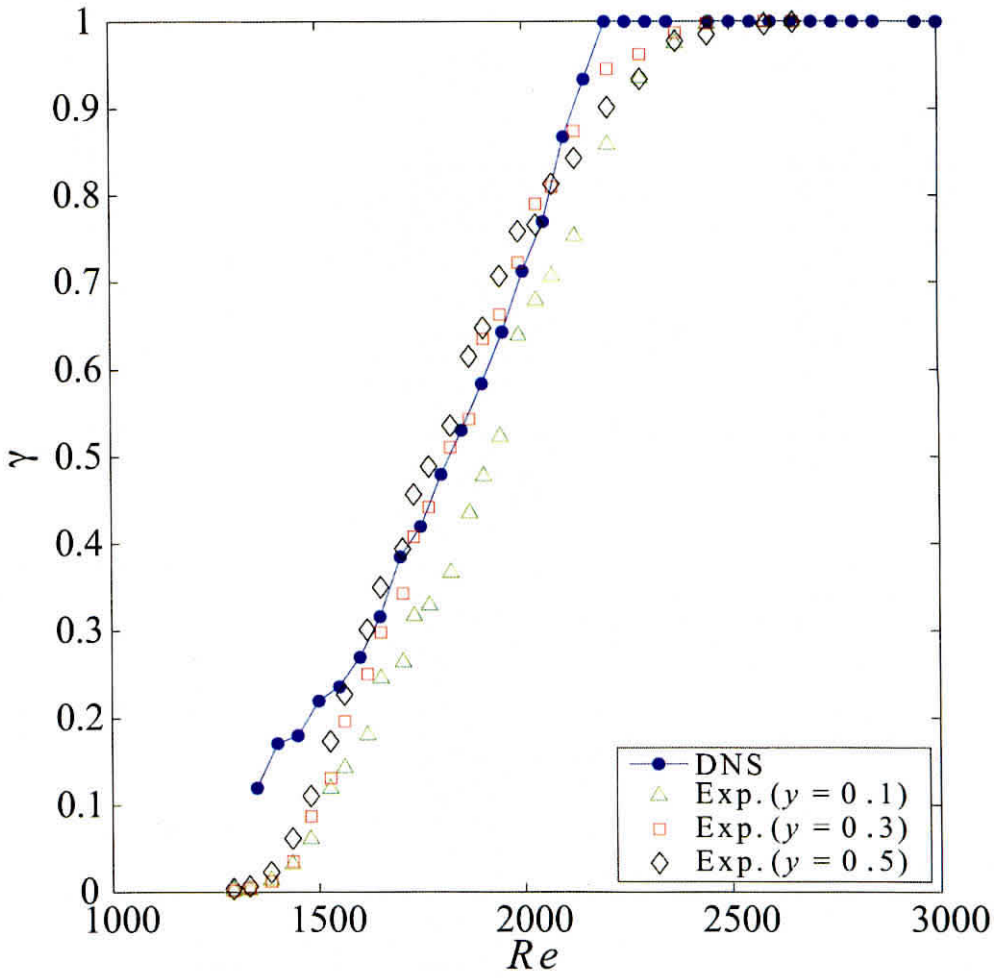

Figure 4.2: Intermittency factor γ vs. Re.

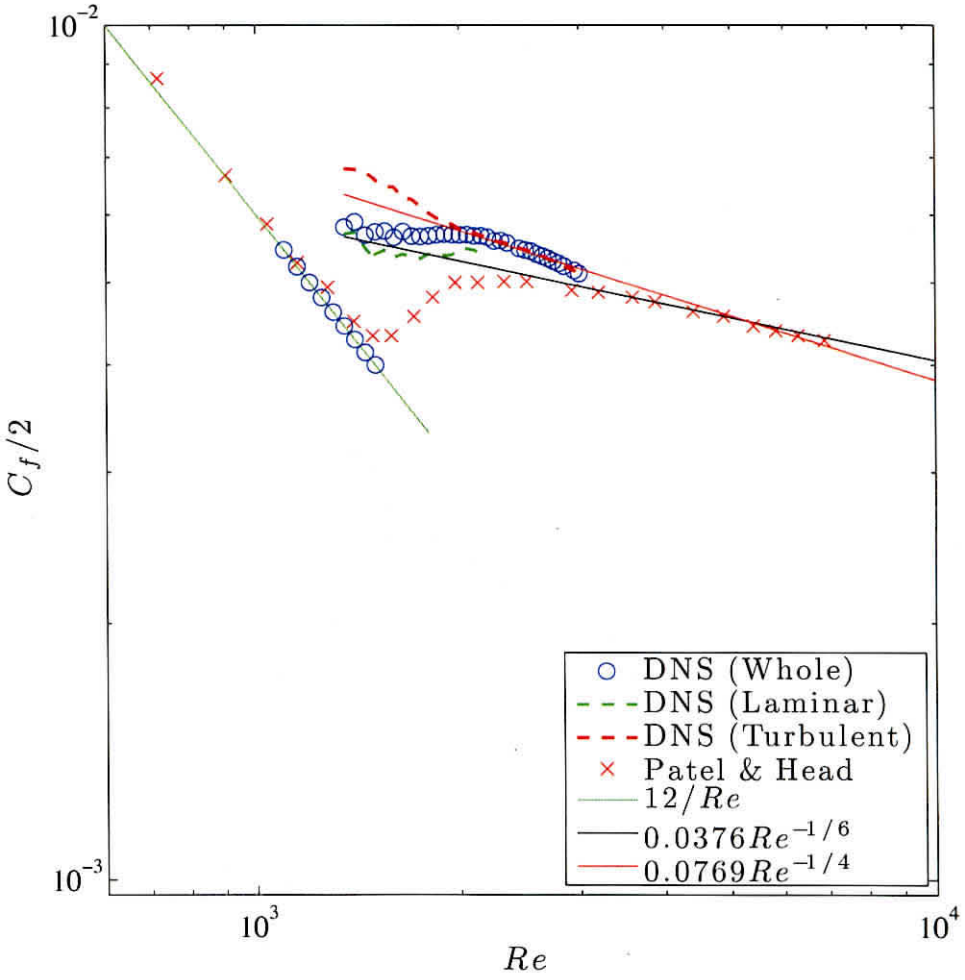

Figure 4.3: Skin friction coefficient, C_f.

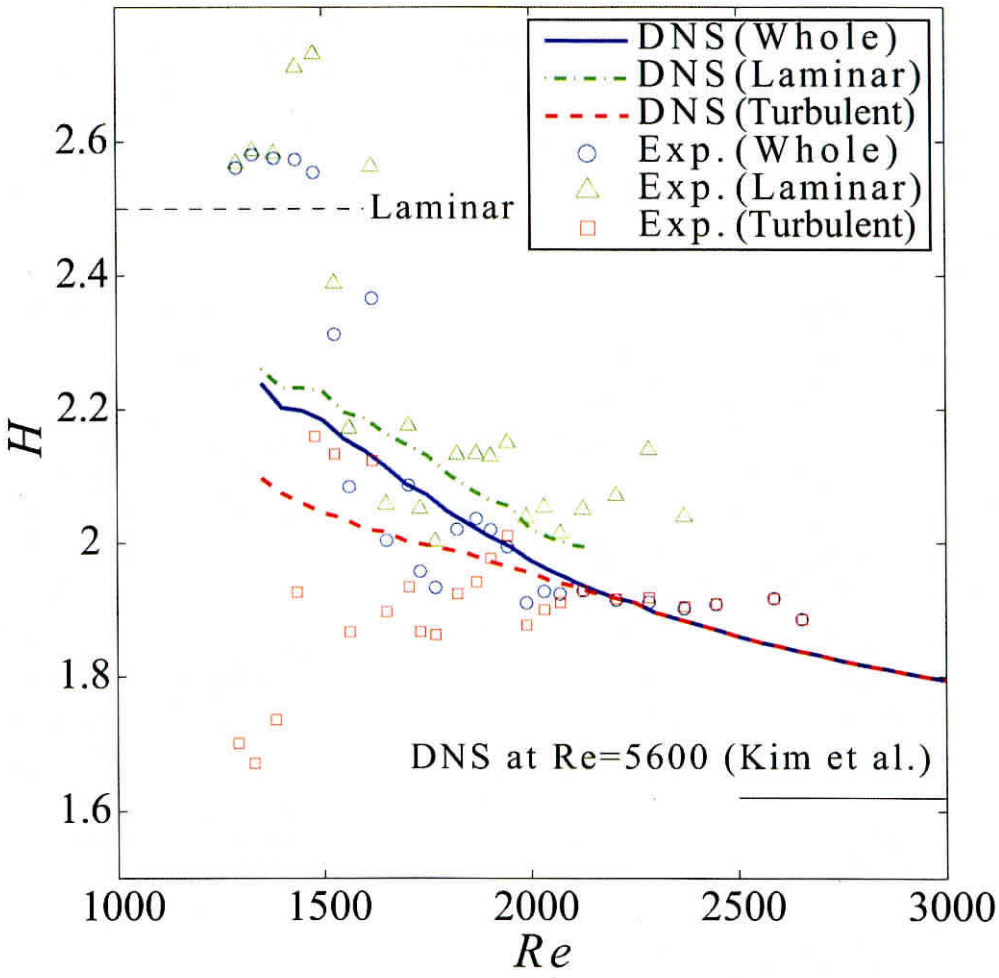

Figure 4.4: Shape factor, H, vs. Re.

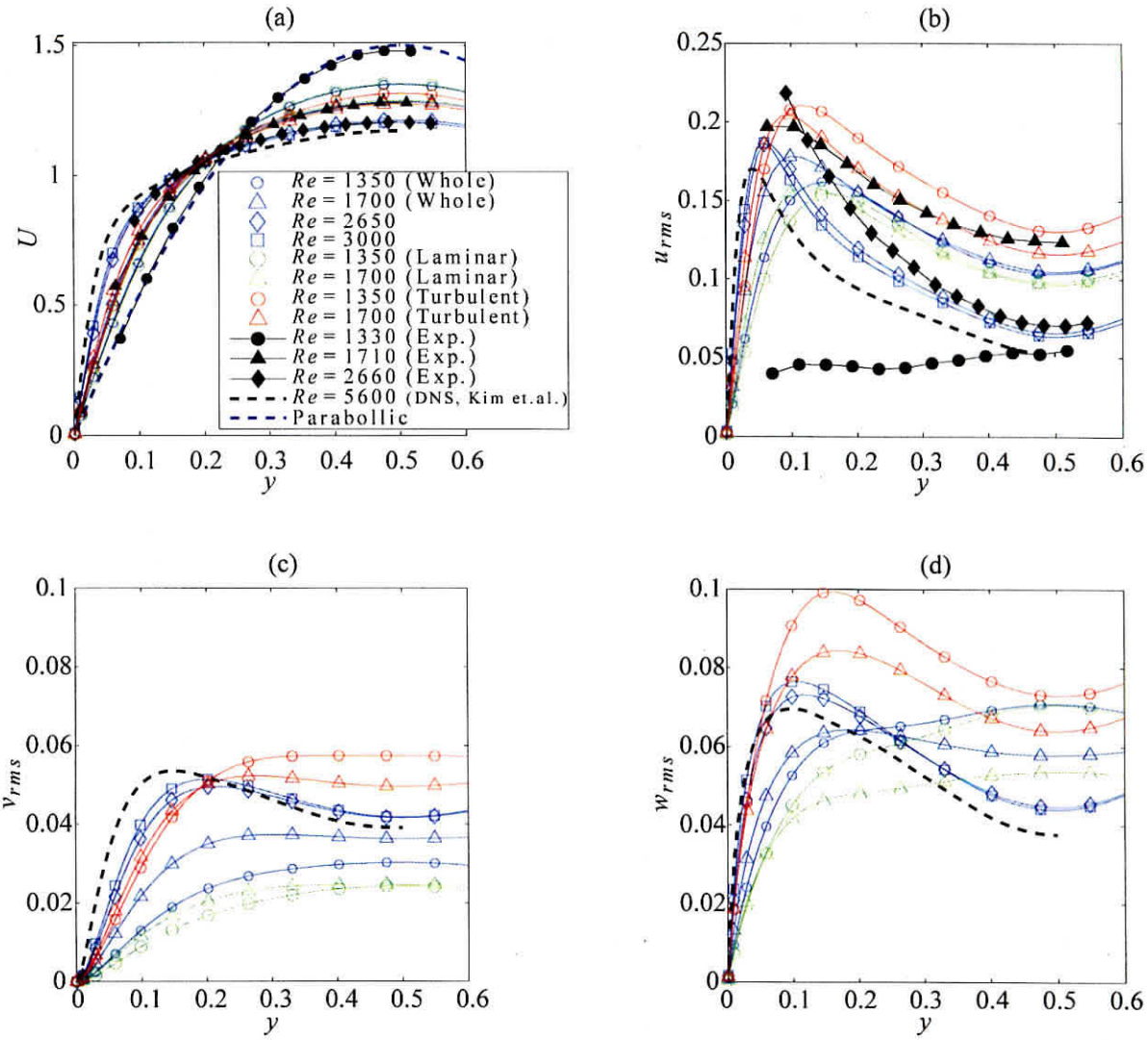

Figure 4.5: Mean velocity profiles and distributions of velocity fluctuations.

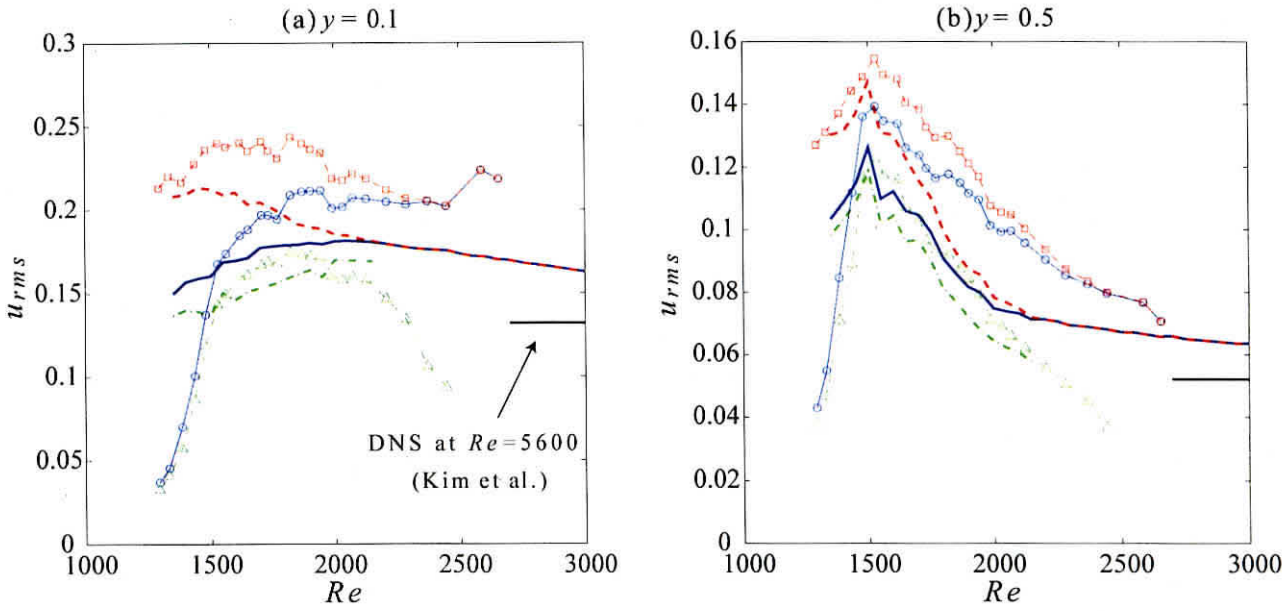

Figure 4.6: Streamwise velocity fluctuations at fixed wall-normal positions, $y = 0.1$ and 0.5. The lines color and symbols are same as in Figure 4.4.

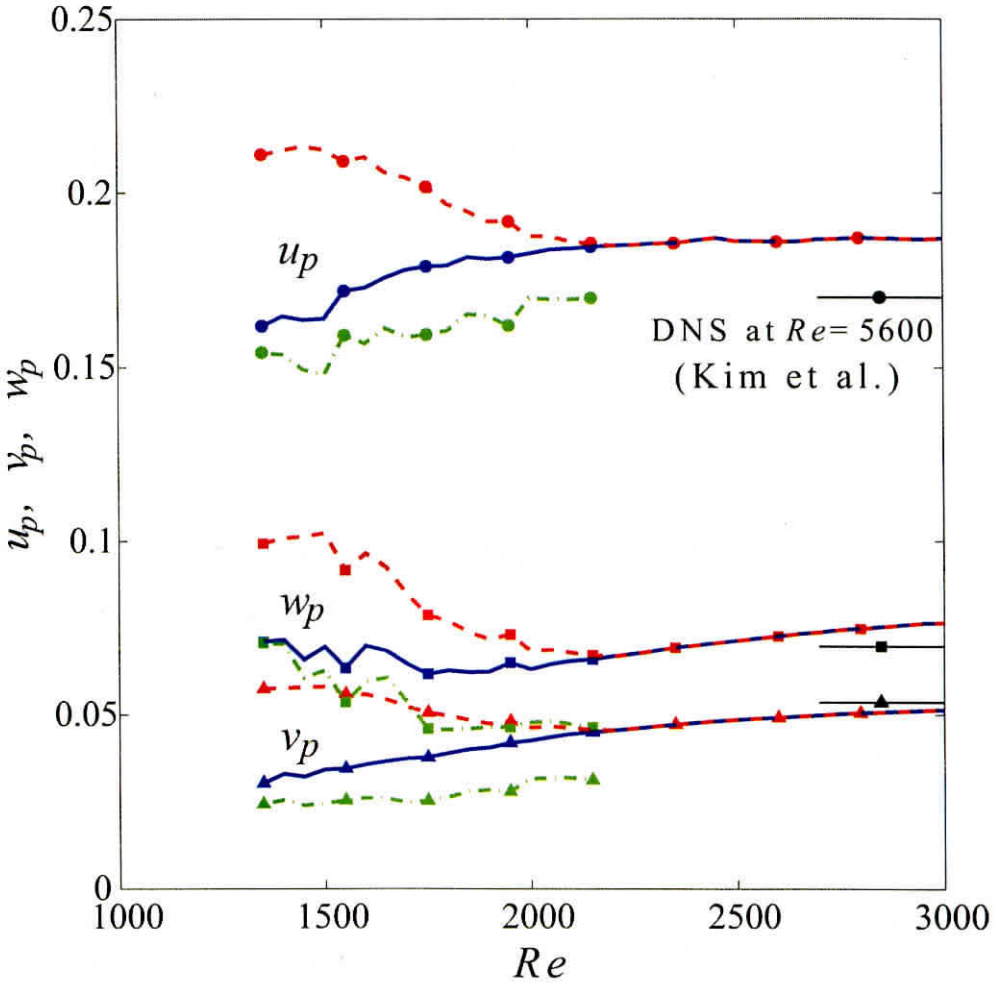

Figure 4.7: Re dependence of the peak values of velocity fluctuations. Lines with circles, triangles and squares are u_p, v_p and w_p, respectively. Color of the lines represents the whole (blue), the turbulent (red) and laminar (green) parts.

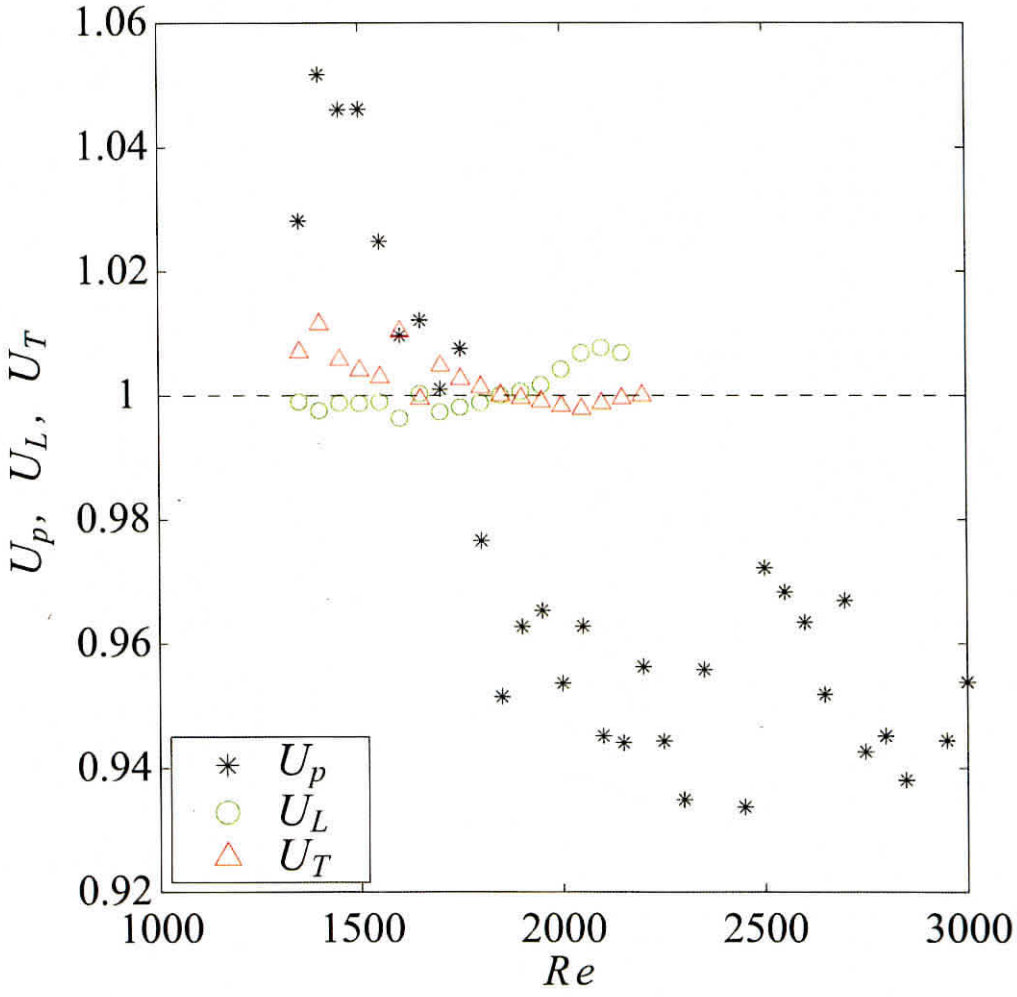

Figure 4.8: Re dependence of patch phase velocity, U_p and the mean velocities, U_L and U_T, of the laminar and turbulent parts.

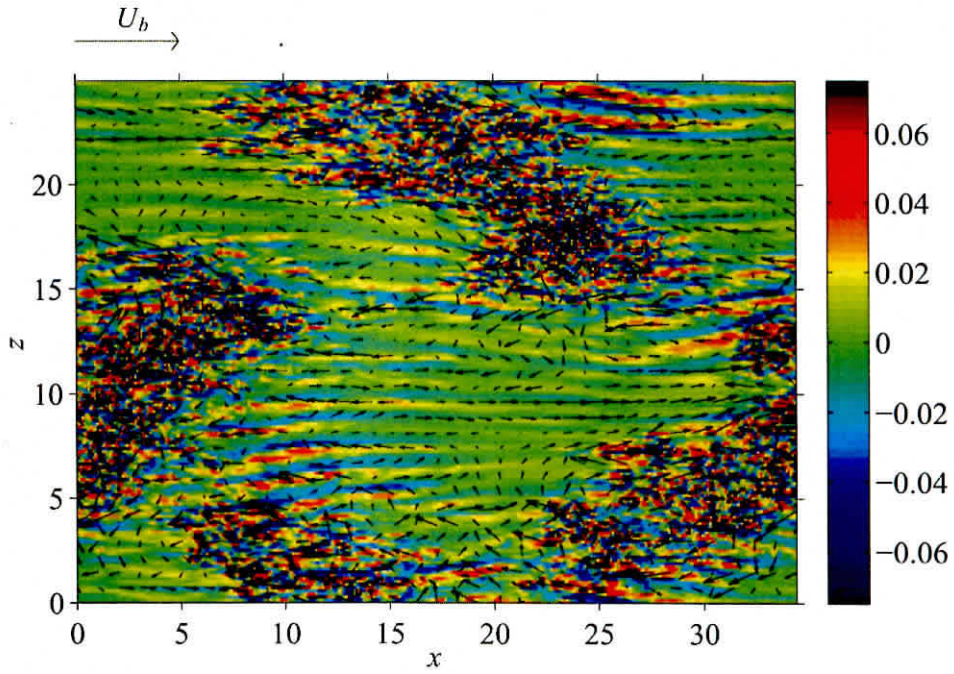

Figure 4.9: A snapshot of the velocity flow field at $Re = 1600$, $y = 0.25$ and $t = 460$. Color image represents the wall-normal velocity fluctuation, v, and arrows represent velocity vectors whose components are the streamwise and spanwise velocity fluctuations, u' and w, respectively.

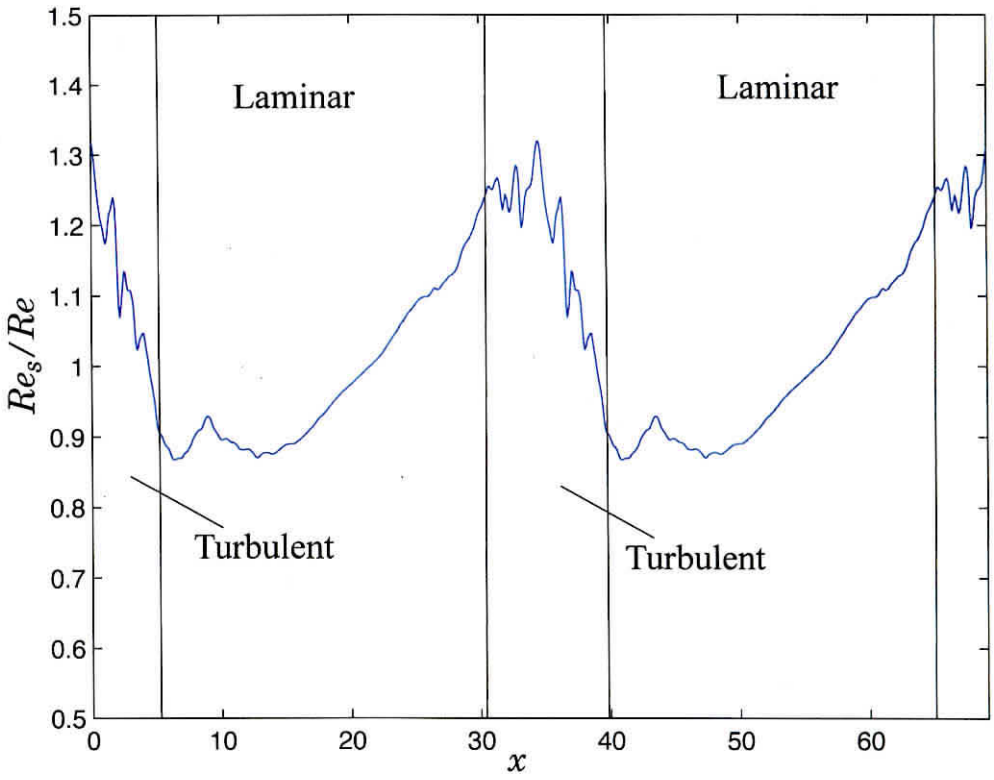

Figure 4.10: Streamwise distribution of the local Reynolds number Re_s at $z = 8.4$ in the snapshot of Figure 4.9.

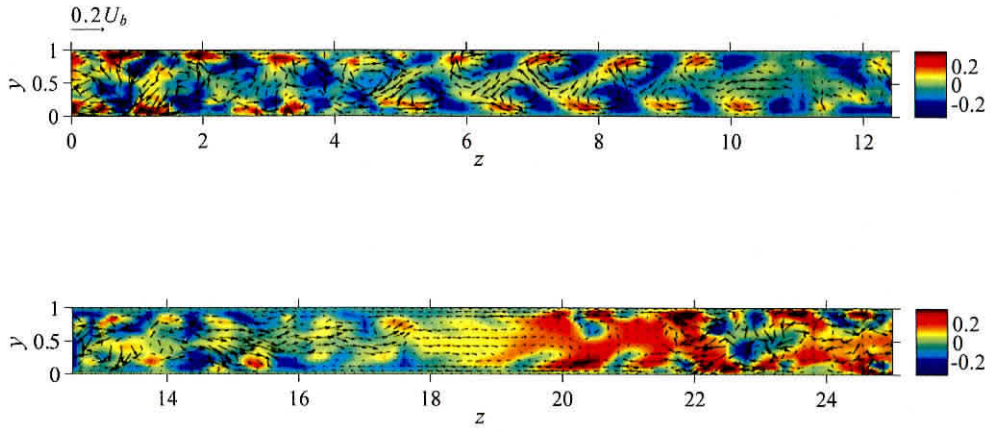

Figure 4.11: A y-z cross section at $x = 10.0$ in the snapshot of Figure 4.9. Color image represents the streamwise velocity fluctuation u', and arrows indicate the wall-normal and spanwise velocity components, v and w, respectively.

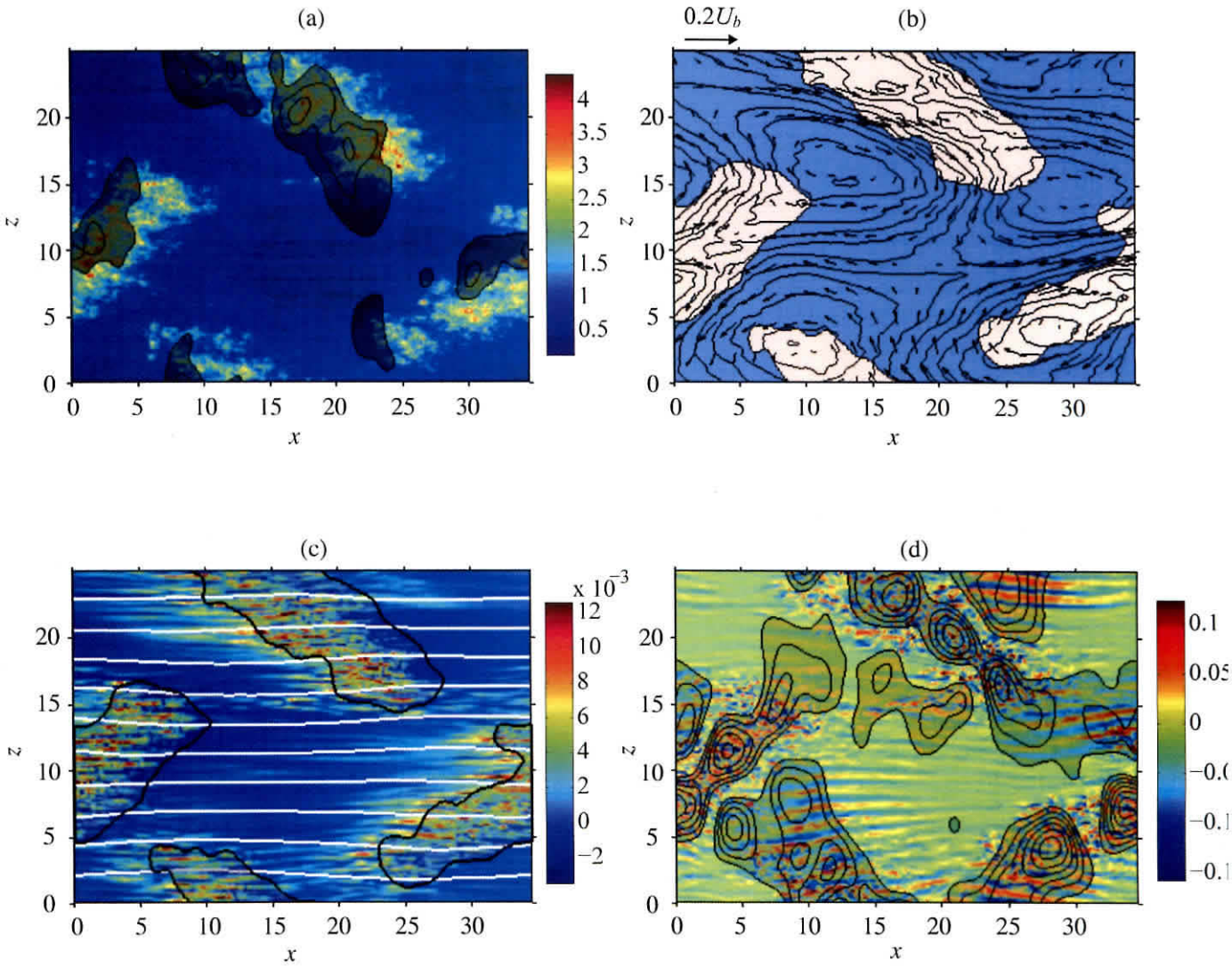

Figure 4.12: Wall-normal Integrated flow field of the snapshot of Figure 4.9. (a) Color image of the detector function, D, and contours of the integrated pressure $\bar{p}$ with contour spacing of 0.005. (b) The relative streamline and the velocity vectors. Pink areas represent the turbulent patches. (c) The local skin friction with the absolute streamlines (white lines). Shaded areas encircled with a black line represent turbulent patches. (d) Color image of the integrated wall normal velocity, $\bar{v}$, and $\partial\bar{w}/\partial x$ with contour spacing of 0.003. Blue and orange shading represents areas of negative and positive curvatures of the absolute streamline, respectively.

CHAPTER 5

Conclusions

The investigations of the transitional channel flow have been described. The main goals of the thesis are to determine the transitional range and to understand the generation mechanisms of the turbulent patch and the streaky structure appeared in the transitional flow.

Transitional range and marginal Reynolds number in channel flow

As seen in Chapter 3 and 4, the transitional range estimated from the variation of intermittency factor is $Re = 1600 - 2000$. The intermittency factor is good index to describe the intermittent flow, but it should be careful to estimate from the statistical information of the flow. The single-slope method was applied to the results of the hot-wire measurements and the DNS. The advantages of this method are avoidance of analyst subjectivity and unique determination of the intermittency factor. Moreover, the threshold value determined by this method was utilized to decompose the flow into laminar and turbulent parts. We also discovered and utilized the 2/3 exponent law for a probability density function of the second streamwise derivative of the velocities in transitional and low-Reynolds-number turbulent flows. Theoretical explanation of this law is still an open question. It

is very interesting why the scaling law is appear at the second derivatives, what the means of the scaling exponent 2/3, and whether this scaling law exist for other intermittent flows, e. g. transitional boundary layer and outer region of turbulent boundary layer etc. The scaling law of probability density function of Burger's turbulence has investigated by many researchers. Attention of the second derivatives, however, is rare to be studied.

The lower marginal Reynolds number is obtained around $Re = 1400$, from neutral growth of streamwise fluctuation energy in relaminarizing channel flow and interpolation of intermittency factor. This value is good agreement with the values from previous workers. However, this value is not excellent agreement with the present DNS result suggesting that more extensive computation is required for the quantification of the transitional range of Reynolds number. Indeed the streamwise fluctuation energy at the most downstream measurement position still increases around the lower marginal Reynolds number. This indicates that there is some possibility to increase the intermittency factor further downstream.

The upper marginal Reynolds number is estimated at $Re = 2600$ from the intermittency factor distribution. The spectra map indicates that the large-scale structure exists above the upper marginal Reynolds number. This fact induces serious problem to treat the flow as homogeneous and it is required that effect of the inhomogeneity should be taken into account for theoretical frameworks.

The generation mechanism of characteristic disturbances in channel flow

In the transitional channel flow, from the analysis of the premultiplied spectra of the velocity fluctuation we confirmed three peaks. One is at very low frequency

that corresponds to the appearance frequency of the turbulent patches and the peak of the high frequency is of the turbulent disturbance. The middle-frequency peak scale appearing for $Re \leq 1800$ at near the wall corresponds to the streaks observed by flow visualization.

The number of turbulent patches is roughly obeyed by the parabolic distribution as a function of the intermittency factor that has the peak at the $\gamma = 0.5$, suggesting that probability of turbulent patch appearance is almost independent of the position.

By means of the ensemble averaging technique based on the laminar-turbulent interfaces, the flow field with a passing turbulent patch was reconstructed. The reconstructed flow field indicates dynamic change of the time-mean velocity profile and the local Reynolds number suggesting that there exist two-dimensional flow structure inside and outside turbulent patches. The wall-normal integrated flow field of the DNS confirmed this large-scale flow structure and revealed the blockage effect of turbulent patches causes it with skewing the streamlines. Appearance of the streaky structures in the laminar part well correlates with the local skewness of the streamlines. This fact strongly suggests that the cross-flow instability induces. As a result of enhancement of the momentum transfer in the wall-normal direction by the streaky disturbances, the mean velocity profile of the laminar part becomes similar to the turbulent one and the skin friction in the lower range of transitional Reynolds number are relatively high in spite of low intermittency factor.

References

[1] S. J. Davies and C. M. White. An experimental study of the flow of water in pipes of rectangular section. *Proc. R. Soc. Lond. A*, 119:92–107, 1928.

[2] M. A. Badri Narayanan. An experimental study of reverse transition in two-dimensional channel flow. *J. Fluid Mech.*, 31:609–623, 1968.

[3] V. C. Patel and M. R. Head. Some observations on skin friction and velocity profiles in fully developed pipe and channel flows. *J. Fluid Mech.*, 38:181–201, 1969.

[4] D. R. Carlson, S. E. Widnall, and M. F. Peeters. A flow visualization study of transition in plane Poiseuille flow. *J. Fluid Mech.*, 121:487–505, 1982.

[5] F. Alavyoon, D. S. Henningsson, and P. H. Alfredsson. Turbulent spots in plane Poiseuille flow-flow visualization. *Phys. Fluids*, 29(4):1328–1331, 1982.

[6] M. Nishioka and M. Asai. Some observations of the subcritical transition in plane Poiseuille flow. *J. Fluid Mech.*, 150:441–450, 1985.

[7] K. Fukudome, O. Iida, and Y. Nagano. Large-scale structure and the sustenance mechanisim in turbulent Poiseuille flow at low Reynolds number. *Trans. JSME, B*, 76:92–107, 2010.

[8] T. Tsukahara, Y. Kawaguchi, H. Kawamura, N. Tillmark, and P. H. Alfredsson. Turbulence stripe in transitional channel flow with/without system rotation. In *Proceedings of the Seventh IUTAM Symposium on Laminar-Turbulent Transition, IUTAM Bookseries, Springer*, volume 18, pages 421–426, 2009.

[9] T. Okumura and M. Matsubara. Experimental study on minimal Reynolds number with LDV measurement and visualization. In *Proc. of 2006 Annual Meeting*, page 42. Japan Society of Fluid Mechanics, 2006.

[10] T. Numano and M. Matsubara. Visualization and LDV measurements of disturbance observation in laminarizing two dimensional channel flow. In *Proc. of 2008 Annual Meeting*, page 29. Japan Society of Fluid Mechanics, 2007.

[11] T. Natori, K. Watanabe, D. Aoki, D. Seki, and M. Matsubara. Flow visualization in a relaminarzing channel flow. In *Proc. 2011 Annual Meeting*, pages 75–76. JSME Hokuriku-Shinetsu Branch, 2011.

[12] J. Kim, P. Moin, and R. Moser. Turbulence statistics in fully developed channel flow. *J. Fluid Mech.*, 177:133–166, 1987.

[13] S. A. Orszag and K. C. Kells. Transition to turbulence in plane Poiseuille and plane Couette flow. *J. Fluid Mech.*, 96:159–205, 1980.

[14] S. Chen and G. D. Doolen. Lattice Boltzmann method for fluid flow. *Ann. Rev. Fluid Mech.*, 30:329–364, 1998.

[15] T. Inamuro. Lattice Boltzmann methods for viscous fluid flows and for two-phase fluid flows. *Fluid Dyn. Res.*, 38:641–659, 2006.

[16] T. Inamuro. A lattice kinetic scheme for incompressible viscous flows with heat transfer. *Phil. Trans. R. Soc. Lond. A*, 360:477–484, 2002.

[17] A. K. M. F. Hussain and W. C. Reynolds. Turbulence statistics in fully developed channel flow at low reynolds number. *J. Fluid Mech.*, 177:133–166, 1987.

[18] Y. Tanaka. Direct numerical simulation of relaminarizing plane-parallel channel flow. Master's thesis, Shinshu Univ., 2004.

[19] J. Peixnho and T. Mullin. Decay of turbulence in pipe flow. *Phys. Rev. Lett.*, 96:094501, 2006.

[20] T. M. Schneider B. Hof, J. Westerweel and B. Eckhardt. Sensitive dependence on initial conditions in transition to turbulence in pipe flow. *Nature*, 443:59–62, 2006.

[21] S. A. Orszag. Accurate solution of the Orr-Sommerfeld stability equation. *J. Fluid Mech.*, 50:689–703, 1971.

[22] O. Iida and Y. Nagano. The relaminarization mechanisms of turbulent channel flow at low Reynolds numbers. *Flow, Turbulence and Combustion*, 60:193–213, 1998.

[23] J. D. Skufcaand, J. A. Yorke, and B. Eckhardt. Edge of chaos in a parallel shear flow. *Phys. Rev. Lett.*, 96:174101, 2006.

[24] T. M. Schneider, B. Eckhardt, and J. A. Yorke. Turbulence transition and the edge of chaos in pipe flow. *Phys. Rev. Lett.*, 99:034502, 2007.

[25] T. M. Schneider, J. F. Gibson, M. Lagha, F. De Lillo, and B. Eckhardt. Laminar-turbulent boundary in plane Couette flow. *Phys. Rev. E.*, 78:037301, 2008.

[26] P. Schlatter Y. Duguet and D. S. Henningson. Localized edge state in plane Couette flow. *Phys. Fluids*, 21:111701, 2009.

[27] T. M. Schneider, J. F. Gibson, and J. Burke. Snakes and ladders: localized solution of plane Couette flow. *Phys. Rev. Lett.*, 104:104501, 2010.

[28] S. Cherubini, P. De Palma, J. Ch. Robinet, and A. Bottaro. Edge state in a boundary layer. *Phys. Fluids*, 23:051705, 2011.

[29] F. Mellibovsky, A. Meseguer, T. M. Schneider, and B. Eckhardt. Transition in localized pipe flow turbulence. *Phys. Rev. Lett.*, 103:054502, 2009.

[30] Y. Duguet, A. P. Willis, and R. R. Kerswell. Transition in pipe flow: the saddle structure on the boundary of turbulence. *J. Fluid Mech.*, 613:255–274, 2008.

[31] Y. Duguet, A. P. Willis, and R. R. Kerswell. Slug genesis in cylindrical pipe flow. *J. Fluid Mech.*, 663:180–208, 2010.

[32] M. Asai and M. Nishioka. Boundary-layer transition triggered by hairpin eddies at subcritical Reynolds numbers. *J. Fluid Mech.*, 297:101–122, 1995.

[33] P. H. Alfredsson and M. Matsubara. Free-stream turbulence, streaky structure and transition in boundary layer flows. *AIAA-paper*, 2000-2534, 2000.

[34] A. V. Johansson and P. H. Alfredsson. On the structure of turbulent channel flow. *J. Fluid Mech.*, 122:295–314, 1982.

[35] B. G. B. Klingmann. On transition due to three-dimensional disturbances in plane Poiseuille flow. *J. Fluid Mech.*, 240:167–195, 1992.

[36] P. T. Tsilingiris. Thermophysical and transport properties of humid air at temperature range between 0 and 100°c. *Energ. Convers. Manage.*, 49:1098–1110, 2008.

[37] T. B. Hedley and J. F. Keffer. Turbulent/non-turbulent decisions in an intermittent flow. *J. Fluid Mech.*, 64:625–644, 1974.

[38] C. L. Kuan and T. Wang. Investigation of the intermittent behavior of transitional boundary layer using a conditional averaging technique. *Exp. Thermal Fluid Sci.*, 1990.

[39] M. Matsubara and P. H. Alfredsson. Disturbance growth in boundary layers subjected to free stream turbulence. *J. Fluid Mech.*, 430:149–168, 2001.

[40] B. G. B. Klingmann and P. H. Alfredsson. Turbulent spots in plane Poiseuille flow – measurements of the velocity field. *Phys. Fluids A*, 2:2183–2195, 1990.

[41] J. P. Monty, J. A. Stewart, R. C. Williams, and M. S. Chong. Large-scale features in turbulent pipe and channel flows. *J. Fluid Mech.*, 589:147–156, 2007.

[42] D. Seki and M. Matsubara. Experimental investigation of relaminarizing and transitional channel flows. *Phys. Fluids*, 24:124102, 2012.

[43] G. Kawahara and S. Kida. Periodic motion embedded in plane Couette turbulence: regeneration cycle and burst. *J. Fluid Mech.*, 449:291–300, 2001.

[44] J. F. Gibson. Channelflow: A spectral Navier-Stokes simulator in C++. Technical report, U. New Hampshire, 2012.

[45] J. F. Gibson, J. Halcrow, and P. Cvitanović. Visualizing the geometry of state space in plane Couette flow. *J. Fluid Mech.*, 611:107–130, 2008.

[46] T. Tsukahara, Y. Seki, H. Kawamura, and D. Tochio. DNS of turbulent channel flow at very low Reynolds numbers. Tsinghua University Press & Springer–Verlag, 2004.